

# The Archean Chalice gold deposit: a record of complex, multistage, high-temperature hydrothermal activity and gold mineralisation associated with granitic rocks in the Yilgarn Craton, Western Australia

Louis A. Bucci<sup>a,\*</sup>, Steffen G. Hagemann<sup>a</sup>, David I. Groves<sup>a</sup>, Jonathan G. Standing<sup>b</sup>

<sup>a</sup>Centre for Global Metallogeny, Department of Geology and Geophysics, University of Western Australia, Nedlands, WA 6907, Australia

<sup>b</sup>Fluid Focus, 23 Milson St., South Perth, WA 6151, Australia

Received 17 November 2000; accepted 25 June 2001

## Abstract

The Chalice gold deposit (~20 t Au produced), in the southwestern portion of the Late-Archean Norseman–Wiluna greenstone belt of the Yilgarn Craton, Western Australia, is hosted both in a sequence of intercalated mafic and ultramafic amphibolites and a post-peak metamorphism monzogranite dike. The deposit is flanked on the western side by calc-alkaline plutonic rocks, and to the east by a predominantly monzogranitic pluton, with at least four generations of monzogranitic dikes that intrude the local mine stratigraphy. Locally, four deformation events (D<sub>1</sub>–D<sub>4</sub>) have affected this sequence of amphibolites, and two stages of gold mineralisation are recognised, controlled by the progressive D<sub>2</sub> event.

Main Stage gold mineralisation (95% of the resource), which is demonstrably later than all granitic bodies except second generation and subsequent monzogranite dikes, is controlled by localised D<sub>2</sub> asymmetric folds developed in the mafic amphibolite. It is expressed as veins and wall-rock replacement, characterised by a prograde assemblage of quartz–diopside–plagioclase–K-feldspar–titanite–pyrrhotite–pyrite–magnetite ± garnet, hornblende, scheelite and biotite. Second Stage gold mineralisation (5% of the resource) is associated with the intrusion of a monzogranite dike and is expressed as disseminated gold in the dike, as well as foliation-discordant veins of quartz–gold, quartz–diopside–gold, actinolite–gold and molybdenite–tellurobismuthite–gold.

Detailed field mapping and petrography suggest that Main Stage gold mineralisation at Chalice is equivalent to hypozonal orogenic lode–gold mineralisation in other Archean greenstone belts of the Yilgarn Craton, whereas monzogranite-associated Second Stage gold mineralisation is atypical of such deposits. The Main Stage mineralisation cannot be correlated to any particular granitoid in the local environment, although temporally, it is bracketed by granitic magmatism. A deep magmatic or metamorphic source cannot be resolved from the field data. It is also uncertain as to whether Second Stage mineralisation represents a true magmatic–gold event, or is a product of the assimilation and remobilisation of Main Stage gold, during the intrusion of the monzogranite dike. However, its distinctive metal association of Au–Bi–Mo–Te–W

\* Corresponding author.

E-mail address: lbucci@geol.uwa.edu.au (L.A. Bucci).

suggests the former. Irrespective of this uncertainty, Chalice remains as a deposit which is more intimately related both spatially and temporally to granitic magmatism than other Yilgarn deposits. © 2002 Elsevier Science B.V. All rights reserved.

*Keywords:* Hypozonal; Orogenic-gold; Monzogranite; Calc-silicate alteration

## 1. Introduction

Many of the larger gold deposits (>1 Moz) of the Archean Yilgarn Craton of Western Australia (Fig. 1) are located in epizonal (e.g. Wiluna: Hagemann et al., 1992) to mesozonal (Golden Mile: Phillips et al., 1996) settings, in the sense of Groves et al. (1998). However, numerous deposits in hypozonal settings (Marvel Loch: Mueller et al., 1991; Corinthia-Frazer's: Bloem et al., 1994; Nevoria: Mueller, 1997) highlight the importance of high metamorphic-grade sequences within greenstone belts with respect to gold production (see review by Ridley et al., 2000).

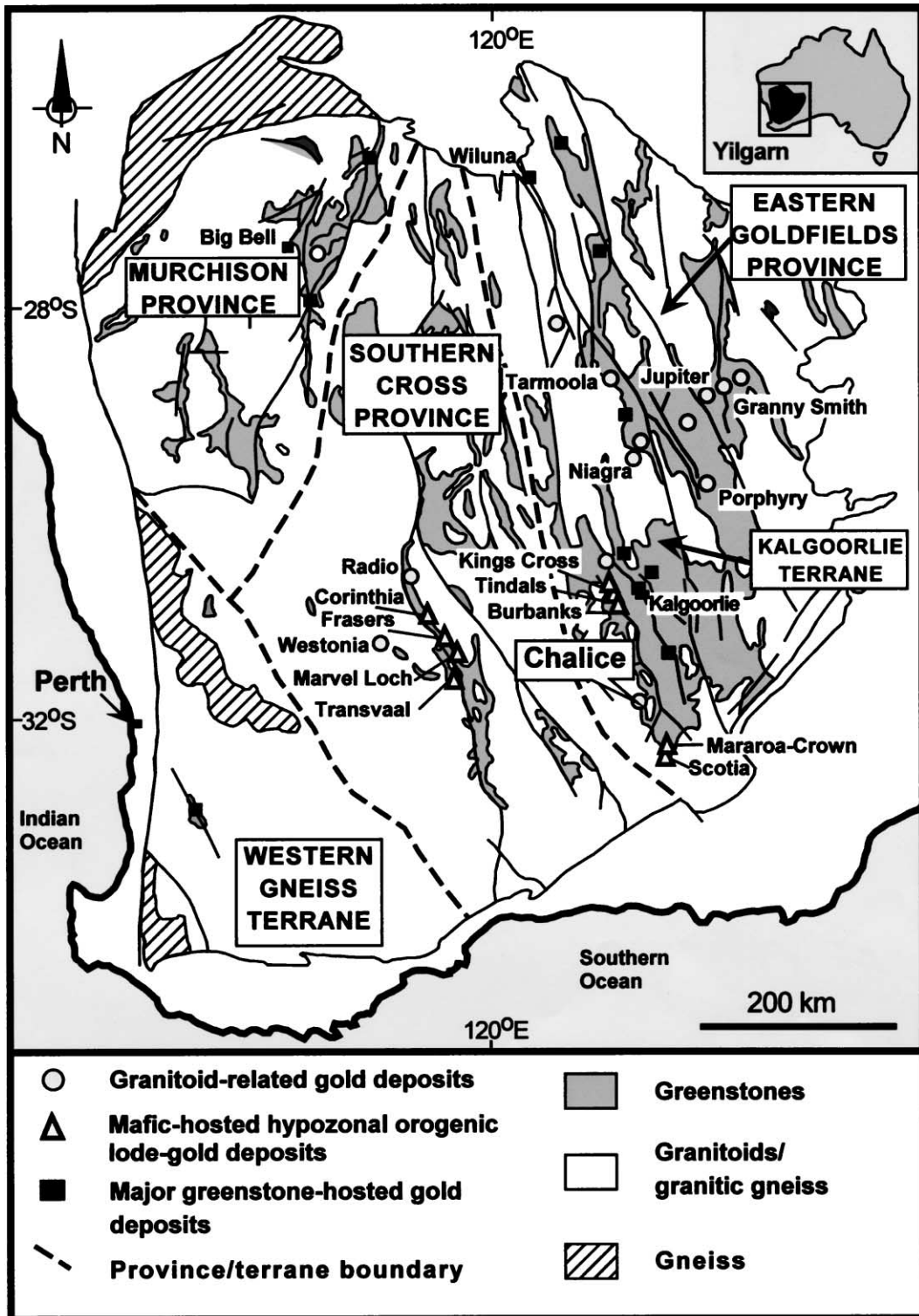
Archean hypozonal orogenic lode–gold deposits in the Yilgarn Craton are characterised by their distinct structural control via ductile shear zones (e.g. Frazers: Barnicoat, 1989; Marvel Loch: Mueller et al., 1991; Corinthia-Hopes Hill: Bloem et al., 1994; Transvaal: Hagemann et al., 1998) with gold hosted in relatively narrow (<3 m) shear veins and associated wallrock alteration zones. High-temperature silicate and sulfide alteration minerals (e.g. diopside, garnet, pyrrhotite) and gold–arsenopyrite–loellingite assemblages characterise the majority of deposits in these settings (Ridley et al., 2000).

The Chalice gold deposit is a 600,000-oz gold deposit located in the Archean Norseman–Wiluna granitoid-greenstone belt, approximately 40 km north-west of the town of Norseman, in the Yilgarn Craton, Western Australia (Fig. 1). The deposit was discovered by the Widgiemooltha Joint Venture (Resolute Samantha 70%, Great Southern Mines 15% and Geographe Resources 15%) via in-fill drilling of a soil sampling programme, which delineated a target area with anomalous gold values peaking at 360 ppb Au

(Bonwick, 1995). The deposit occurs in a mid- to upper-amphibolite facies domain, is spatially and temporally related to granitic rocks, and is characterised by high-temperature silicate and sulfide alteration assemblages (e.g. diopside, garnet and pyrrhotite, respectively), not dissimilar to deposits of the high metamorphic grade Southern Cross Province (e.g. Frazers: Barnicoat, 1989; Marvel Loch: Mueller et al., 1991; Corinthia-Hopes Hill: Bloem et al., 1994; Transvaal: Hagemann et al., 1998) to the west (Fig. 1). This suggests that Chalice may belong to the hypozonal suite of orogenic lode–gold deposits, in the sense of Groves et al. (1998). However, Chalice has some atypical structural features and mineralisation styles relative to the majority of other documented deposits in amphibolite facies domains (e.g. Ridley et al., 2000). These anomalous features must be understood before Chalice can be used in a more generic sense, as the genetic classification of gold deposits hosted in amphibolite facies terranes is a contentious issue (Mueller et al., 1991, 1996; Groves, 1993; Bloem et al., 1994; Knight et al., 2000). Groves (1993) suggests that hypozonal deposits form as part of a continuum of deposits, over an extended range of crustal conditions, that form from deeply sourced metamorphic fluids. However, Mueller et al. (1996) argue that the high-temperature wall-rock alteration assemblages and gold mineralisation in these deposit types are the result of the interaction of granitoid-derived magmatic fluids.

The spatial and temporal association of gold mineralisation with granitic rocks at Chalice provides an excellent opportunity to document the effect of direct interaction between granitic rocks and gold deposits in hypozonal settings. The objective of this paper is,

Fig. 1. Geological map of the Yilgarn Craton in Western Australia, showing the location of the Chalice gold deposit and some major greenstone-hosted lode–gold deposits including selected hypozonal orogenic lode–gold deposits and granitoid-hosted gold deposits. Modified after Cassidy et al. (1998).



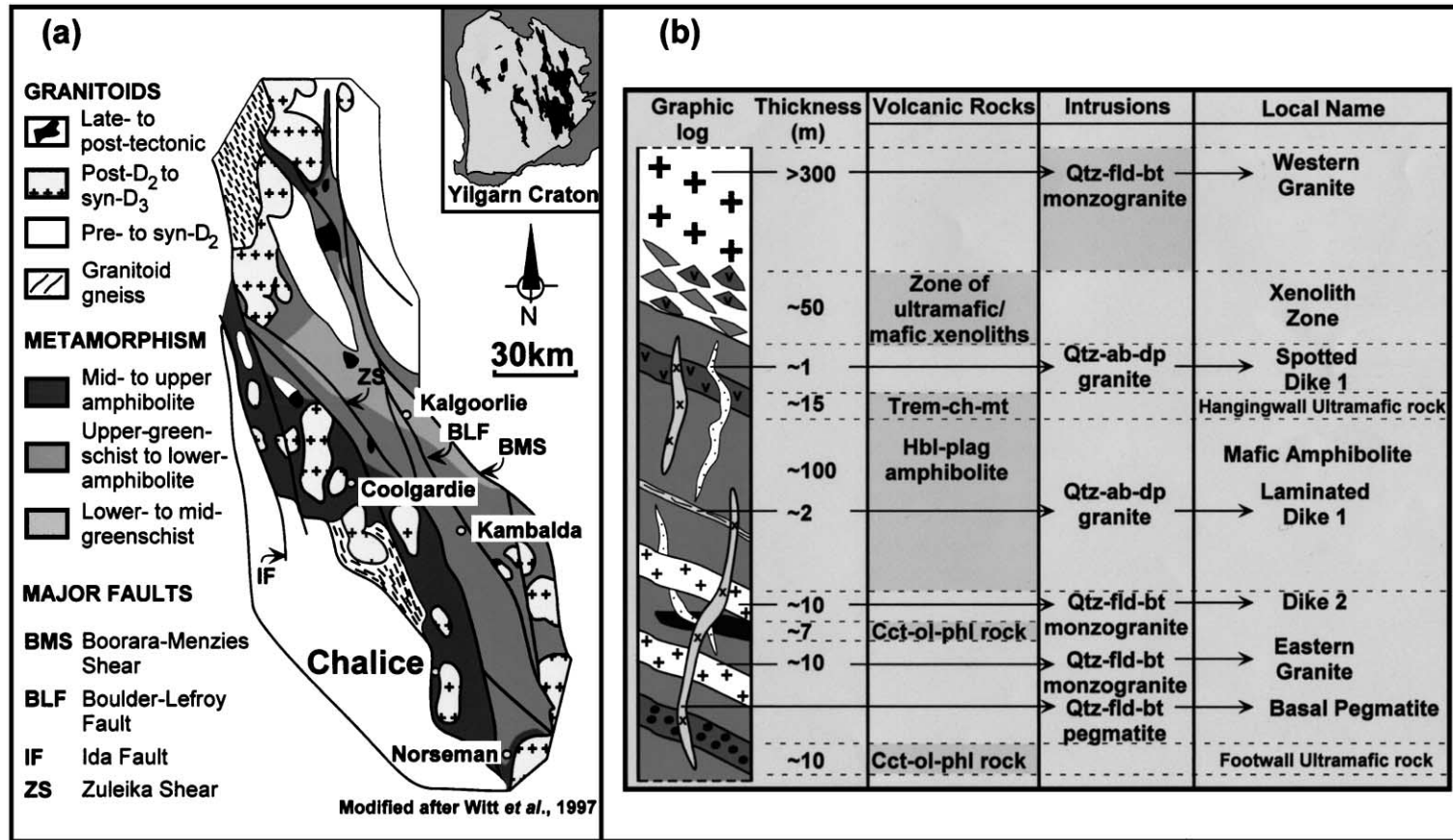


Fig. 2. (a) Regional geology of the southwestern portion of the Norseman-Wiluna greenstone belt. Inset shows the Yilgarn Craton and the distribution of greenstone belts within it. (b) Sequence of lithologies at the Chalice gold mine.

therefore, to describe the lithostratigraphic, structural, mineralisation and alteration characteristics of the complex Chalice gold deposit. A descriptive model based on relative timing relationships is proposed in an attempt to contribute towards a resolution of the controversy surrounding the genesis of orogenic lode-gold deposits in hypozonal settings.

## 2. Regional geology

The Archean Yilgarn Craton of Western Australia is subdivided into five superterranes, each of which is an amalgamation of smaller terranes (Fig. 1; Myers, 1997). The Chalice gold deposit is located in the south-western portion of the Kalgoorlie Terrane, which is one of the five terranes (Gindalbie, Jubilee, Kurnalpi, Kalgoorlie and Norseman) that make up the Eastern Goldfields Superterrane (Myers, 1997).

The Kalgoorlie Terrane is a north–northwest-trending Archean greenstone belt, characterised by a consistent, strike-extensive stratigraphy, comprising a lower mafic–ultramafic sequence overlain by felsic volcanic and volcanoclastic rocks (Swager et al., 1992). Depositional ages for the greenstones based on SHRIMP U–Pb in zircon data range from 2700–2690 Ma for the mafic–ultramafic sequence to ~2680 Ma for the felsic volcanic sequence (Claoué-Long et al., 1988; Nelson, 1995). Recent dates in overlying sedimentary sequences suggest deposition of felsic detritus up to ~2650 Ma (Krapez et al., 2000). This supracrustal sequence is intruded or bounded by numerous granitoid bodies, encompassing three periods of magmatism. Voluminous granitoid emplacement occurred at 2690–2685 and 2665–2660 Ma with less-widespread intrusive activity at 2630–2600 Ma (Campbell and Hill, 1988; Hill et al., 1992).

Models for the regional deformation systematics of the Eastern Goldfields Superterrane have been proposed by many workers (e.g. Hammond and Nisbet, 1992; Swager et al., 1992; Myers, 1993, 1997; Williams and Whitaker, 1993; Archibald, 1998). Despite variations between models, it is generally accepted that the tectonic evolution of the Eastern Goldfields Superterrane involved four major periods of regional-scale deformation. Regional deformation of the greenstones commenced with south-over north-

directed thrust faulting and recumbent folding ( $D_1$ ). Predominantly east–northeast compression during  $D_2$  resulted in the formation of upright folds with north–northwest-trending fold axes and associated faults. Subsequent west–southwest-directed compression ( $D_3$ ) produced strike–slip and subvertical movement on regional shear zones. East–west compression during  $D_4$  resulted in limited oblique to lateral displacement across north–northeast- and southeast-striking faults. The metamorphic grade of the terrane ranges from lower greenschist facies in the central low-strain section to mid- to upper-amphibolite facies along the western margin of the terrane and surrounding post- $D_2$  to syn- $D_3$  granitoids (Myers, 1997). Thus, high-grade metamorphism is generally considered to be broadly syn- $D_3$ .

The Chalice deposit is located in a 2–3-km-wide sequence of alternating mafic and ultramafic rocks in the southwestern, high-metamorphic grade portion of the Kalgoorlie Terrane (Fig. 2a). It is flanked on the western side by the calc-alkaline granitic rocks of the Woolgangie Supersuite (ca. 2646 Ma; Hill et al., 1992) and on the eastern side by the predominantly monzogranitic Pioneer Dome (ca. 2665–2655 Ma; Nelson, 1995). East-vergent folds at the Chalice deposit are interpreted to be associated with the western limb of a regional antiform ( $F_4$  fold of Archibald et al., 1978), likely developed during the diapiric emplacement of the Pioneer Dome (see Archibald, 1979).

## 3. Lithostratigraphic, magmatic and metamorphic setting of the Chalice gold deposit

### 3.1. Introduction

The lithostratigraphic sequence of the Chalice gold deposit comprises NNW-striking and W-dipping intercalated mafic and ultramafic rocks that are metamorphosed to mid-amphibolite facies grade. This sequence is bounded to the west by the eastern margin of the calc-alkaline Woolgangie Supersuite granitoids, which are exposed in the western wall of the Chalice open pit, and to the east by the intrusive contact of the monzogranitic Pioneer Dome batholith. Four generations of granitic dike cross-cut the lithostratigraphic sequence and can be temporally

differentiated based on cross-cutting relationships between dikes and fabrics developed in the volcanic units and by the degree of hydrothermal alteration that they have experienced.

### 3.2. Lithostratigraphy

All mafic and ultramafic rocks in the lithostratigraphic succession have been metamorphosed to mid-amphibolite facies. The present mineralogy of the rocks represents a combination of regional amphibolite-facies metamorphism and gold-related hydrothermal alteration. The following descriptions of mafic and ultramafic rocks relate to the least-altered protoliths exposed at Chalice.

#### 3.2.1. Mafic rocks

The dominant unit is a fine-grained, weakly to strongly foliated amphibole–plagioclase amphibolite, which is regionally extensive and can be traced throughout the Chalice open pit and underground workings. The unit is up to 100 m thick and is intercalated with thin (<20 m) alternating ultramafic units lower in the sequence (Fig. 2b). It consists of hornblende (50%), plagioclase (40%), quartz (8%)

and trace ilmenite. The texture of the rock is lepidoblastic, characterised by aligned grains of hornblende alternating with plagioclase–quartz-rich domains. Major and trace element geochemistry (Table 1) indicates that this unit is tholeiitic in composition.

#### 3.2.2. Ultramafic rocks

There are two major and one minor ultramafic units at Chalice. These units are discontinuous throughout the open pit and underground workings, but can be traced throughout the deposit. The first ultramafic unit, locally termed the Hangingwall Ultramafic Unit (Fig. 2b), marks the westernmost boundary of gold mineralisation. This unit is a fine- to medium-grained, moderately to strongly foliated tremolite–chlorite rock, which is up to 15 m thick. It is composed of tremolite (70%) and chlorite (20%) with trace magnetite and weakly serpentinised relict olivine. Mineralogically similar, discontinuous thin slivers (<5 m) of ultramafic rock are also distributed throughout the sequence.

The second ultramafic unit, locally termed the Footwall Ultramafic Unit (Fig. 2b), marks the easternmost boundary of gold mineralisation, and is also up to 15 m thick. It is a medium-grained, moderately

Table 1

Representative whole-rock analyses of least-altered mafic and ultramafic rocks at the Chalice gold mine

UWA no.	Mafic rocks		Ultramafic rocks		
	Mafic amphibolite	Mafic amphibolite	Hangingwall ultramafic	Footwall ultramafic	Calcite–olivine–phlogopite rock
	Chal 24	Chal 25	Chal 26	Chal 27	Chal 15
SiO <sub>2</sub> (wt.%)	49.34	51.06	52.01	51.71	23.04
TiO <sub>2</sub>	1.30	1.42	0.30	0.33	0.90
Al <sub>2</sub> O <sub>3</sub>	12.83	14.01	6.15	6.99	1.77
Fe <sub>2</sub> O <sub>3</sub>	17.41	14.51	11.15	11.35	22.05
FeOt	15.66	13.06	10.03	10.21	19.84
MgO	7.84	5.37	21.51	20.28	31.14
MnO	0.24	0.29	0.20	0.21	0.49
CaO	8.84	10.15	7.14	8.01	20.52
Na <sub>2</sub> O	1.84	1.88	0.51	0.13	0.04
K <sub>2</sub> O	0.24	1.16	1.02	0.99	0.05
P <sub>2</sub> O <sub>5</sub>	0.12	0.15	0.02	0.01	0.01
LOI	0.33	1.14	1.74	1.80	17.13
CO <sub>2</sub> (%)	0.11	0.15	0.15	0.22	14.69
S	0.24	0.30	0.03	0.05	0.55
Total	100.8	99.76	99.48	99.79	98.63

NB: Representative analyses presented are based on geochemical analysis of five samples for each sample type.

to strongly foliated tremolite–olivine rock, composed of tremolite (60%), variably serpentinised olivine (20%), chlorite (15%) and trace magnetite. Both the Hangingwall and Footwall Ultramafic units exhibit a lepidoblastic texture defined by preferentially aligned tremolite grains. Major and trace element geochemistry (Table 1) indicates that they are komatiitic in composition.

There is also a minor, discontinuous ultramafic unit up to 5 m thick at Chalice. It is a coarse to medium-grained granoblastic rock, composed of calcite (50%), phlogopite (20%) and olivine (15%) with accessory hornblende and magnetite. Intercalated slivers of this unit (<1 m thick) towards the base of the sequence are generally associated with basaltic komatiite. Major and trace element geochemistry (Table 1) indicates that this unit is a komatiite as classified by Arndt and Nisbet (1982) although definitive textures are lacking.

### 3.2.3. Granitic rocks

Five granitic rock types have been identified at Chalice including four generations of granitic dikes which intrude the lithostratigraphic sequence. These dikes can be temporally differentiated on the basis of mutual cross-cutting relationships and their timing with respect to fabrics developed in the volcanic sequences. The other granitic rock at Chalice is locally termed the Western Granite (Fig. 2b). It is a medium to coarse-grained rock composed of quartz (40%), plagioclase (20%), orthoclase (20%) and biotite (15%) with accessory magnetite and titanite. Towards its footwall contact, the Western Granite displays a weak gneissic fabric (up to 10 m wide) defined by crudely aligned biotite grains alternating with domains of feldspar and quartz. This localised 10 m zone is interpreted to represent deformation of the Western Granite, associated with its emplacement, rather than recrystallisation during metamorphism. Numerous variably altered xenoliths of mafic and ultramafic volcanic rocks also characterise the footwall margin of the Western Granite and define a ~50-m-wide zone, locally termed the Xenolith Zone (Fig. 2b). The Western Granite is interpreted to have been emplaced late in the deposit evolution, syn- to post-dikes and post-gold mineralisation based on three main criteria.

1. The footwall contact with the volcanic units is strongly sheared, and a gneissic fabric charac-

terises the footwall zone of the Western Granite. This contact does not have the calc-silicate alteration that characterises the Chalice ore body, as described below.

2. Mafic xenoliths do, however, display the same alteration assemblage (calc-silicate) as the altered mafic amphibolites of the Chalice ore-body; yet, the granite is not calc-silicate altered.
3. This granite is not mineralised.

The first dikes to have intruded the sequence are locally termed Spotted Dike 1 and Laminated Dike 1 (Fig. 2b). Spotted Dike 1 is a fine to medium-grained rock, which has been strongly hydrothermally altered to its present mineralogy. It consists of granoblastic plagioclase (albite–oligoclase 70%) and quartz (15%) with porphyroblastic diopside (10%) and trace actinolite and titanite. Laminated Dike 1 is composed of fine-grained granoblastic plagioclase (albite–oligoclase, 70%), quartz (20%) and accessory disseminated diopside, actinolite, titanite, pyrite and pyrhotite. Discontinuous laminae of coarse-grained diopside, and chlorite after actinolite, characterise this unit and differentiate it from the mineralogically similar Spotted Dike 1. These dikes display no mutual cross-cutting relationships and cannot be temporally differentiated. Spotted and Laminated Dike 1 truncate the primary fabric developed in the volcanic rocks, are extensively hydrothermally altered relative to the other dikes and are cut by all other dikes, indicating that they were the first dikes to intrude the sequence. Gold grades for both Laminated and Spotted Dike 1 are generally less than 0.2 ppm.

Dike 2 (Fig. 2b) is a medium- to coarse-grained monzogranite which consists of quartz (40%), plagioclase (25%), orthoclase (20%) and biotite (10%) with accessory magnetite and titanite. A weak biotite-defined foliation parallels the margins of this dike and is developed for up to 1 m into it. This dike trends generally parallel to the primary fabric developed in the volcanic units; however, it truncates this fabric by up to 30° in the mineralised zone within in mafic amphibolite. In this intersection zone, trace coffinite, uraninite, sphalerite and galena are associated with moderate development of chlorite after biotite, and gold grades within the dike exceed 30 g/t. Dike 2 truncates Dike 1 and is subsequently cross-cut by the

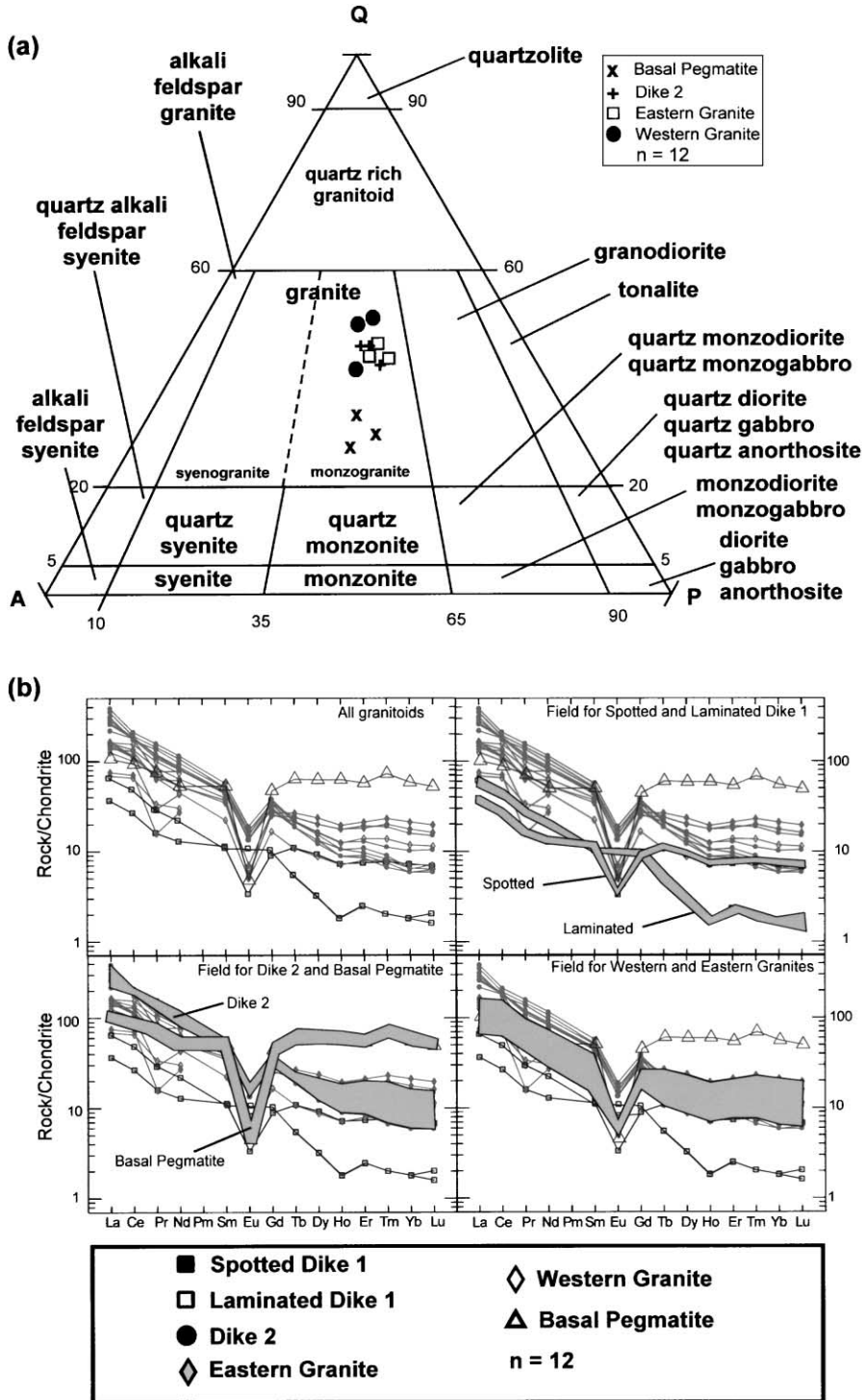


Fig. 3. (a) I.U.G.S. classification for plutonic rocks and (b) REE plots for granitic rocks in the vicinity of the Chalice gold deposit.



last two granitic dike phases, indicating that it is the second dike to intrude the sequence.

The third dike at Chalice is locally termed the Eastern Granite (Fig. 2b) and is a medium-grained rock composed of quartz (40%), plagioclase (25%), orthoclase (20%) and biotite (10%) with accessory magnetite. This dike trends parallel to the primary fabric developed in the volcanic units, truncates both

Dike 1 and Dike 2 and contains no gold mineralisation (<0.02 ppm).

The last dike to have intruded the sequence is locally termed the Basal Pegmatite (Fig. 2b). This flat-lying dike truncates the primary fabric in the volcanic units and all other granitic rocks at Chalice. It is a coarse-grained to pegmatitic rock composed of quartz (30%), orthoclase (30%), plagioclase (30%) and

Table 2  
Representative whole-rock analyses of least-altered granitic rocks at the Chalice gold mine

	Spotted Dike 1	Laminated Dike 1	Dike 2	Dike 2	Western granite	Western granite	Eastern granite	Eastern granite	Basal pegmatite
UWA no.	Chal 2	Chal 3	Chal 4	Chal 9	98969147A (AGSO)	98969147B (AGSO)	Chal 12	Chal 13	Chal 16
<i>Major elements (wt.%)</i>									
SiO <sub>2</sub>	66.12	73.57	74.76	75.24	75.67	74.94	75.69	75.47	67.65
TiO <sub>2</sub>	0.05	0.08	0.21	0.14	0.06	0.15	0.10	0.10	0.28
Al <sub>2</sub> O <sub>3</sub>	17.41	14.55	13.77	13.69	13.67	13.34	13.31	13.45	14.53
Fe <sub>2</sub> O <sub>3</sub>	1.48	0.70	1.81	1.55	0.50	0.99	1.26	1.12	3.63
FeOt	1.33	0.63	1.63	1.40	0.45	0.89	1.13	1.01	3.26
MgO	0.34	0.11	0.35	0.34	0.30	0.44	0.23	0.22	2.21
MnO	0.05	0.05	0.04	0.03	0.01	0.01	0.02	0.01	0.11
CaO	3.34	0.74	1.61	1.30	0.47	0.21	0.69	0.63	1.79
Na <sub>2</sub> O	11.01	7.16	4.75	4.08	5.23	3.66	3.89	3.53	4.39
K <sub>2</sub> O	0.08	2.80	2.64	3.57	3.20	5.28	4.78	5.40	5.22
P <sub>2</sub> O <sub>5</sub>	0.14	0.03	0.06	0.05	0.02	0.03	0.04	0.06	0.19
LOI	2.05	ND	0.67	0.51	ND	ND	0.58	0.59	1.56
CO <sub>2</sub> (%)	1.98	ND	0.15	0.15	ND	ND	0.18	0.15	0.77
S (%)	0.33	0.02	0.08	0.04	0.02	0.03	0.03	0.05	0.24
Total	100.34	99.84	98.99	100.99	99.25	99.25	100.59	100.72	100.8
<i>Trace elements (ppm)</i>									
Ba	111	32	818	871	682	828	315	300	189
Rb	55	1	211	200	206	205	249	248	281
Sr	34	62	133	154	87	131	58	64	75
Pb	7	12	77	75	72	75	77	72	12
Th	7	6	42	41	53	51	31	25	50
U	5	4	21	18	38	11	65	16	83
Zr	17	30	173	169	148	150	62	54	48
Nb	30	14	16	18	5	6	9	7	31
Y	18	16	32	34	16	13	29	20	133
La	5	9	52	63	33	39	18	17	34
Ce	18	16	110	114	80	95	43	39	78
Nd	9	6	36	39	29	35	13	14	31
V	4	5	6	8	6	4	4	2	33
Cr	0	77	2	137	2	2	0	0	272
Ni	0	5	0	34	4	0	0	0	42
Cu	0	23	0	5	0	0	25	15	5
Zn	18	127	40	60	45	44	14	13	36
Ga	23	34	19	24	17	17	17	18	21

NB: Representative analyses presented are based on geochemical analysis of five samples for each granite type.

biotite (5%) with accessory magnetite. Gold grades are generally below 0.02 ppm.

All granitic rocks at Chalice are petrographically classified as granite to monzogranite according to the Streckeisen (1976) I.U.G.S classification of plutonic rocks (Fig. 3). The granitic rocks (Table 2, Fig. 3a) display generally similar trends in major oxides, trace and rare earth elements, suggesting that they belong to the same magmatic suite. The largest relative variation in major and trace element geochemistry between the granitic rocks is displayed by Laminated Dike 1, which has been strongly metasomatised, with enrichment of  $\text{Na}_2\text{O}$ ,  $\text{CaO}$  and depletion in  $\text{K}_2\text{O}$  due to albitisation of feldspars (Fig. 3b). The Basal Pegmatite also displays a relative variation compared to other granitic rocks with a strong enrichment in heavy rare earth elements (Fig. 3b, Table 2).

### 3.3. Metamorphism

The least-altered mafic and ultramafic rocks are characterised by peak-metamorphic assemblages of hornblende–plagioclase and tremolite–chlorite, respectively. Both rock types display a well-developed peak-metamorphic fabric defined by lepidoblastic amphiboles, which have been deformed in subsequent deformation events. These equilibrium assemblages are indicative of mid-amphibolite facies metamorphism (Winkler, 1976) and, based on hornblende–plagioclase geothermobarometry in the mafic amphibolites, yield peak-metamorphic temperatures and pressures between  $490 \pm 25$  and  $530 \pm 25$  °C and 3–5 kbar (Fig. 4). These  $P$ – $T$  estimates correspond to a range of crustal depths between  $\sim 12$  and 14 km (Miyashiro, 1973).

### 3.4. Relative timing of metamorphism and magmatism

The peak-metamorphic fabric in mafic and ultramafic rocks is defined by lepidoblastic amphiboles, which delineate a moderate to well-developed foliation throughout the volcanic units. All granitic dikes at Chalice truncate this peak-metamorphic fabric and retain their igneous textures, indicating that their emplacement or intrusion was post-peak-metamorphic in timing. The Western Granite was emplaced along the western margin of the lithostratigraphic sequence

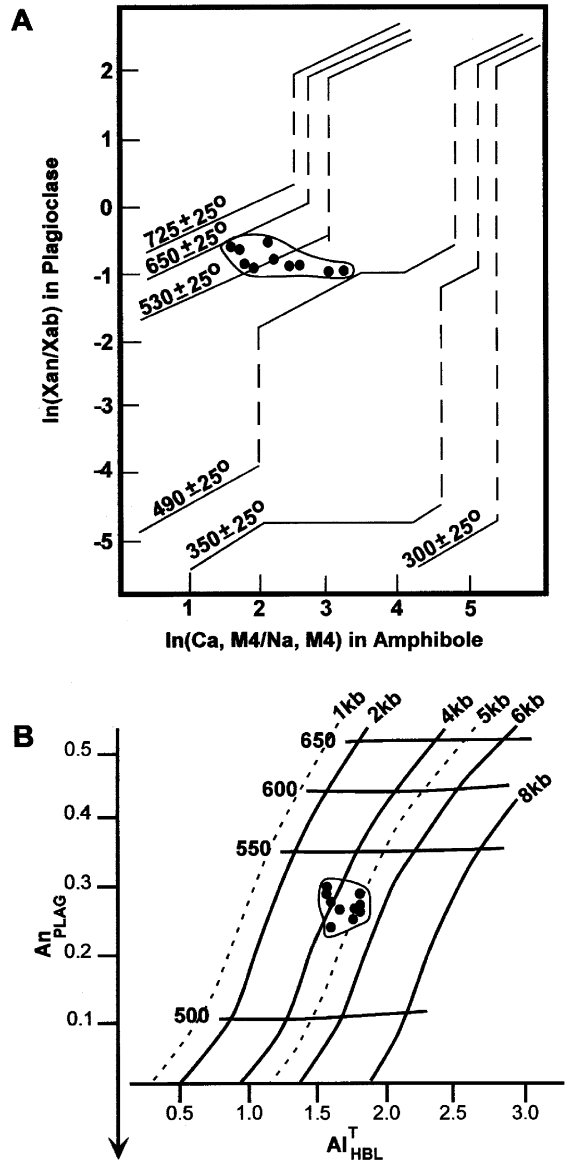


Fig. 4. Calculated pressure–temperature estimates for peak-metamorphic conditions at the Chalice gold deposit. Samples plotted are of amphibole–plagioclase pairs in least-altered mafic amphibolite. (A) Plot of  $\ln(\text{Ca}, \text{M4}/\text{Na}, \text{M4})$  in amphibole vs.  $\ln(\text{Xan}/\text{Xab})$  in plagioclase. Geothermometer after Spear (1980). (B) Plot of  $\text{Al}_{\text{HBL}}^{\text{T}}$  in amphibole vs. anorthite content of plagioclase. Thermobarometric grid after Plyusnina (1982).

with the contact generally parallel to the peak-metamorphic fabric developed in the volcanic units. The mafic and ultramafic xenoliths, which comprise the

Xenolith Zone of the Western Granite, retain their peak-metamorphic fabric. Furthermore, the Western Granite displays an igneous granitic to pegmatitic texture, which suggests that it was emplaced during post-peak-metamorphism conditions, not prior to their development.

## 4. Structural setting and orebody geometry

### 4.1. Introduction

The Chalice ore environment is characterised by four transitional deformation events (Fig. 5). Fabrics associated with each deformation event can be temporally differentiated based on cross-cutting relationships mapped in the open pit, underground workings and in drillcore. In the following section, deformation events and associated generated structures are discussed with respect to the nomenclature of Bell and Duncan (1978).

### 4.2. Deposition of greenstones—bedding

This event is relatively unconstrained at Chalice. Lithological contacts and peak-metamorphic fabrics in the mafic and ultramafic volcanic rocks have parallel orientations, dipping  $\sim 70^\circ \rightarrow 261^\circ$ . Lithological contacts are consistently gradational, conformable and are not fault bound. Therefore, the  $S_0$  form surface can be tentatively defined by the lithological contacts of the volcanic units. However, lack of spinifex texture or pillow structures in the volcanic units precludes the assignment of young direction to the sequence.

### 4.3. $D_1$ event

The  $D_1$  event at Chalice is interpreted to have produced the pervasive foliation  $S_1$  ( $\sim 70^\circ \rightarrow 261^\circ$ ; Fig. 5), which can be continuously traced throughout the deposit, is regionally extensive, and corresponds to the regional  $D_2$  event (e.g. Myers, 1993, 1997). This pervasive foliation, assigned  $S_1$ , is parallel to the interpreted  $S_0$  form surface, implicating transposition of  $S_0$  and  $S_1$  ( $S_{0-1}$ ). However,  $S_1$  is used to avoid confusion with respect to nomenclature in subsequently generated fabrics. The  $S_1$  foliation is defined by lepidoblastic amphiboles which alternate with

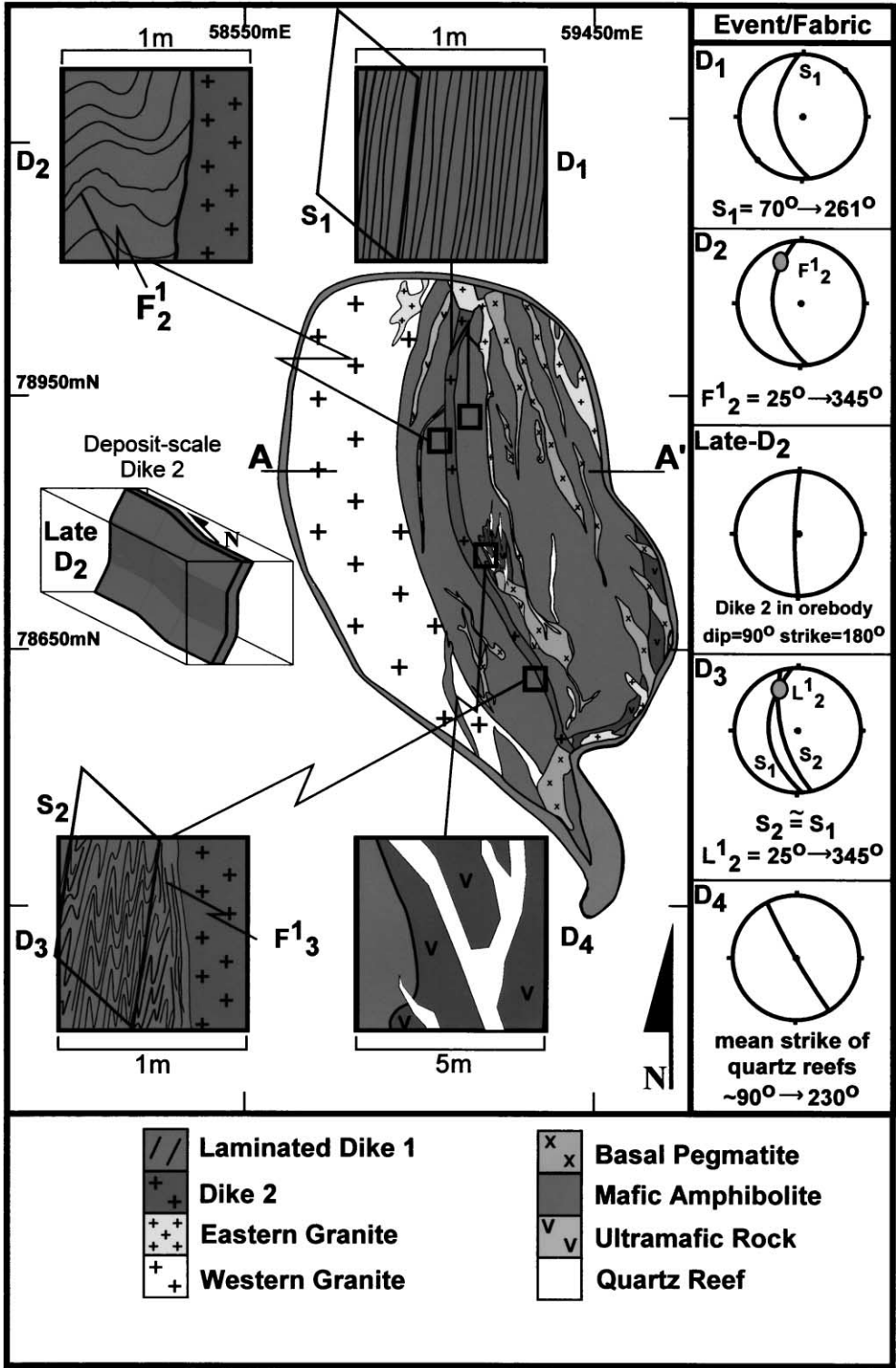
domains of recrystallised plagioclase and quartz. This fabric corresponds to the peak-metamorphic fabric documented for this portion of the greenstone belt (Morris, 1993).

### 4.4. $D_2$ event

The  $D_2$  event at Chalice is represented by local east-verging asymmetric folds ( $F_2^1$ ) that plunge  $\sim 25^\circ \rightarrow 345^\circ$  (Fig. 5). The local development of these folds in a thin ( $< 50$  m) section of the mafic amphibolite, coupled with the asymmetric nature of the folds, indicates localised strain partitioning in the mafic amphibolite. At the regional scale, the folds are likely related to the emplacement of the Pioneer Dome and represent east-vergent S-folds on the western limb of a regional  $F_4$  anticline (in the sense of Archibald, 1979). At a deposit scale, these folds are interpreted to represent a relict, failed, broad ductile shear zone although penetrative shear fabrics, such as S–C fabrics and mylonitisation, are not developed. Foliation ( $S_1$ )-parallel gold-bearing veins, described in more detail below, are locally folded, attenuated and boudinaged during the  $D_2$  event. High-grade shoots plunge parallel to  $F_2^1$  fold axes and indicate an inherent relationship between gold mineralisation and the  $D_2$  event.

### 4.5. Late $D_2$

The development of  $F_2^1$  folds was interrupted by the late  $D_2$  intrusion of a monzogranite dike (Dike 2), which clearly cross-cuts these folds (Fig. 5). The dike intrudes parallel to the  $S_1$  foliation, except where it truncates the  $F_2^1$  folds in the orebody. In section, the dike reflects a sinistral jog-like geometry, which contrasts with the dextral jog-like geometry for the dike along strike (Fig. 5). The interference zone of these opposing jog geometries coincides with the 6 g/t gold Chalice orebody, developed predominantly in the mafic amphibolite (Fig. 6a). Extensive disseminated gold mineralisation is also developed throughout the dike in this interference zone. Foliation ( $S_1$ )-discordant gold-bearing veins are spatially associated with the Dike 2 monzogranite and interpreted to represent veins developed in accommodation of the intrusion of the dike into the sequence. They are only developed on the hangingwall side of Dike 2 and the gold



endowment from these veins contributes <5% to the overall gold budget of the deposit.

#### 4.6. $D_3$ event

This event is interpreted to represent the continuation of the  $D_2$ -folding event, post-intrusion of Dike 2, and produced tight-to-isoclinal folds ( $F_3^1$ ) that plunge parallel to  $F_2^1$  fold axes, and are best developed at the margin of Dike 2 (Fig. 5). An associated axial-planar cleavage ( $S_2$ ), oriented approximately  $60^\circ \rightarrow 270^\circ$ , was developed during this progressive event and is only locally developed towards the hangingwall contact of Dike 2 with the amphibolite. The intersection of  $S_1$  and  $S_2$  produced an intersection lineation  $L_2^1$  oriented approximately  $25^\circ \rightarrow 345^\circ$ .

#### 4.7. $D_4$ event

The final deformation event, recognised at Chalice, produced massive quartz reefs and open-space cavity quartz growth. The massive quartz reefs are up to 30 m, but average approximately 15 m, in width. The reefs preferentially transect the footwall ultramafic unit in the southern end of the deposit; however, they do extend north along strike and intersect the mafic amphibolite and Dike 2 at depth. They dip variably between vertical and  $80^\circ W$ , strike approximately  $350^\circ$ , and contain no gold mineralisation. They are interpreted to reflect exhumation and uplift of the sequence.

#### 4.8. Ore body geometry

Gold mineralisation at Chalice forms a  $\sim 45 \times 170 \times 300$  m grossly stratabound ore body which grades 6 g/t gold and dips  $\sim 70^\circ$  towards  $261^\circ$ , parallel to the  $S_1$  foliation. The ore body is predominantly hosted in the mafic amphibolite with high-grade zones located within, and at the contact of, Dike 2 (Fig. 6a). In a longitudinal projection, the Chalice ore body delineates two main trends (Fig. 6b). High-grade (200–400 gm) shoots are only locally developed and plunge moderately towards the NNW. The

plunges of these shoots are parallel to, and controlled by, the fold axes of  $F_2^1$  and  $F_3^1$  folds, which plunge  $\sim 25^\circ \rightarrow 345^\circ$ . Medium-grade (50–200 gm) gold mineralisation exhibits a gentle southerly plunge, controlled by the intersection of  $S_1$ -conformable mineralisation ( $\sim 70^\circ \rightarrow 261^\circ$ ) with Dike 2 (oriented  $\sim 90^\circ \rightarrow 360^\circ$  in the ore body) to give a deposit-scale plunge for the ore body of  $\sim 18^\circ \rightarrow 182^\circ$ . Low-grade (10–50 g) background mineralisation is developed with no particular orientation, outside the influence of  $F_2^1$  and  $F_3^1$  folds and Dike 2. The absence of these structures and Dike 2 is interpreted to have precluded the development of high fluid flow and wall-rock interaction and, hence, resulted in only a low concentration of gold.

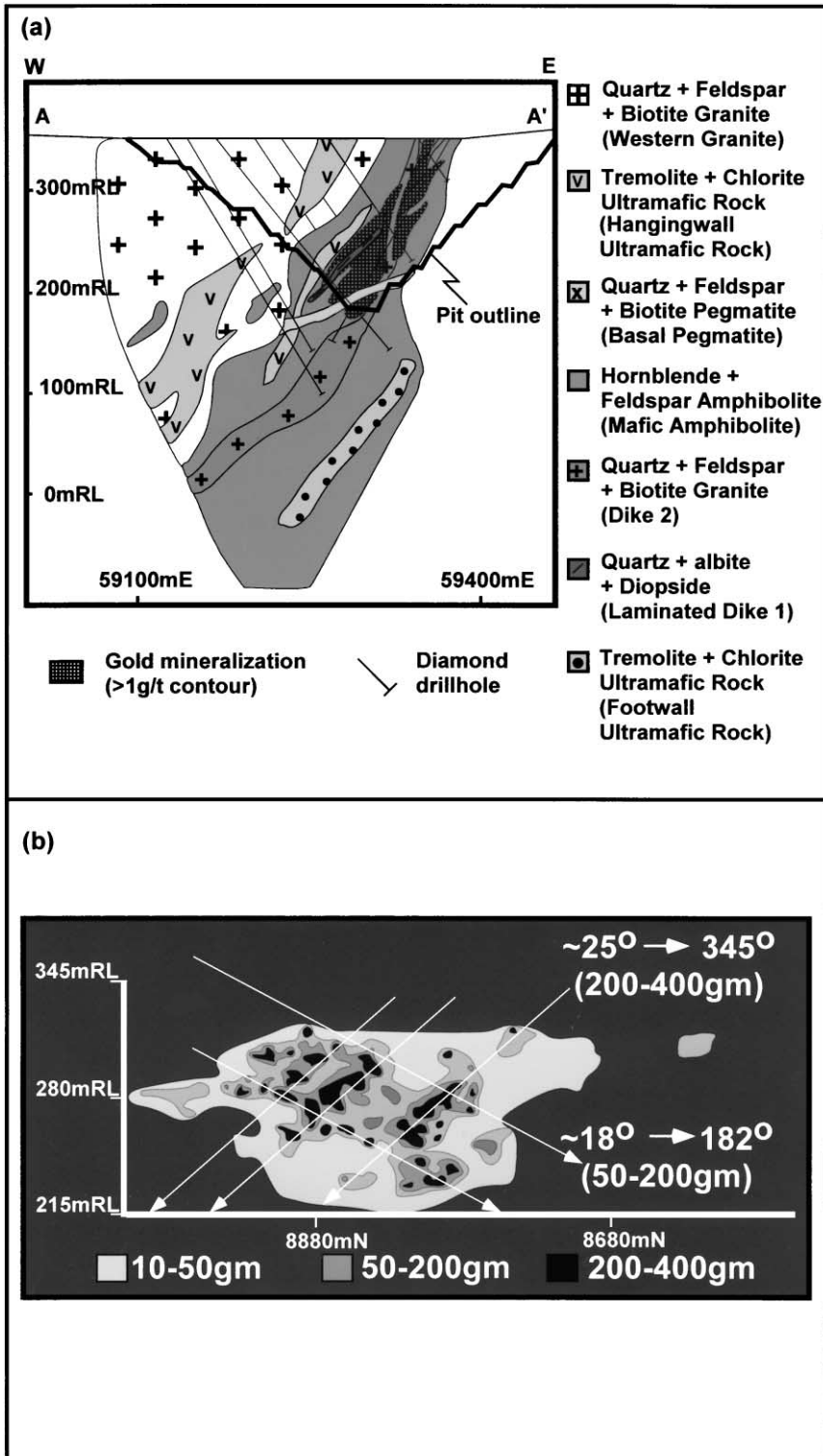
#### 4.9. Structural timing of gold mineralisation

There appear to be two distinct gold mineralisation events at Chalice. The majority of the gold (>95%) is hosted exclusively in the mafic amphibolite, in  $S_1$ -parallel veins and in pervasive wall-rock alteration that replaces metamorphic minerals defining the  $S_1$  foliation. This is termed Main Stage gold mineralisation. Veins are variably deformed and range from folded to boudinaged to essentially undeformed.

Several features indicate a broadly syn- to post-peak metamorphic timing for Main Stage gold mineralisation, coevaluated with the formation of  $F_2^1$  folds during the  $D_2$  event. These are:

1. The lack of intense penetrative fabrics in  $S_1$ -parallel veins. This suggests a minimum timing of post  $D_1$  (hence, post-peak metamorphism) for gold-bearing veins.
2. The replacement of the peak-metamorphic fabric ( $S_1$ ), defined by amphibole-plagioclase, with gold-bearing pervasive wall-rock alteration.
3. The plunge of high-grade shoots parallel to the axes of  $D_2$  and  $D_3$  folds. This suggests an inherent relationship between  $D_2$ -folding (post-peak metamorphism) and gold mineralisation.

Fig. 5. Simplified open pit geology map of the Chalice gold deposit displaying the distribution of the structures including fabrics, organised in terms of the sequence  $D_1$  to  $D_5$ .



4. The presence of monomineralic amphibole vein selvages, which overprint the peak-metamorphic fabric and are in optical discontinuity with peak-metamorphic amphiboles.
5. The occurrence of gold as inclusions and intergrowths in textural equilibrium with high-temperature alteration minerals in veins and pervasive wall-rock alteration.

Points 1, 3 and 5 are discussed below in the section on hydrothermal alteration.

A Second Stage of mineralisation, contributing <5% of the overall gold endowment for the entire orebody, is represented by disseminated gold in Dike 2 and by foliation-discordant quartz–gold, amphibole–gold, pyroxene–gold and molybdenite–gold veins. Foliation-discordant veins are exclusively developed on the hangingwall side of Dike 2, generally within ~10 m of the contact. As both Dike 2 and these veins truncate the  $S_1$  fabric and Main Stage mineralisation, Second Stage mineralisation is also interpreted to be post-peak-metamorphism in timing. The Main and Second Stage mineralisation styles are described in more detail below.

## 5. Main Stage gold mineralisation

### 5.1. Introduction

Two styles of gold mineralisation are recognised in the Main Stage mineralisation at the Chalice gold deposit (Fig. 7): (a) gold-bearing calc-silicate veins and (b) pervasive calc-silicate wall-rock alteration with disseminated gold. Textural and petrological descriptions of these styles are given below with representative microprobe analyses of the alteration minerals in Table 3.

### 5.2. Analytical methods

Microprobe analyses of silicate minerals were carried out at the Centre for Microscopy and Micro-

analysis at the University of Western Australia, using a JEOL JSM 6400 scanning electron microscope (SEM) fitted with a Link EDS X-ray analysis system. Major elements were determined at an accelerating voltage of 15 kV, a specimen current of 5 nA and a live counting time of 60 s. The silver content of native gold was analysed at an accelerating voltage of 20 kV, a specimen current of 3 nA and a live counting time of 60 s.

### 5.3. Overview of Main Stage calc-silicate veins

The most voluminous style of gold mineralisation is  $S_1$ -parallel gold-bearing calc-silicate veins (Fig. 7a), which are sporadically distributed, but hosted exclusively in the mafic amphibolite, and vary with respect to their degree of deformation (folded to boudinaged to essentially undeformed) and their size (1 to 30 cm wide). Calc-silicate veins are characterised by a prograde assemblage of quartz – diopside – plagioclase – K-feldspar – titanite  $\pm$  garnet  $\pm$  hornblende  $\pm$  scheelite and biotite. Accessory pyrite, pyrrhotite and magnetite are also common. However, the development of these veins does not everywhere equate to gold mineralisation, as the same generation veins are not everywhere gold enriched. The representative modal mineralogy and paragenetic sequence for Type 1 veins are presented in Fig. 8.

### 5.4. Type 1 veins

Type 1 veins occur only in the mafic amphibolite, are oriented parallel to the  $S_1$  foliation ( $\sim 70^\circ \rightarrow 261^\circ$ ) and vary from 1 to 30 cm thick and from undeformed to strongly boudinaged and folded. This vein type is variably mineralised (<0.1 ppb to 50 g/t gold) and is not restricted to the 1 g/t gold Chalice orebody envelope (Fig. 6a). Type 1 veins are typically composed of quartz (25%), albite (25%), diopside (20%), titanite (20%), pyrrhotite (3%) and gold (2%) with trace scheelite, pyrite, magnetite, chalcopyrite and rare calcite and apatite (Fig. 7b). Garnet is sporadically developed, but generally constitutes up

Fig. 6. (a) Geological cross-section through the 8800 mN of the Chalice orebody. (b) Longitudinal projection of gold grade  $\times$  thickness in the plane of the Chalice orebody, showing grade distribution in the mafic amphibolite.





## Pervasive alteration

UWA no.	WMD61-7 Titanite	WMD61-7 Andradite	WMD61-7 Andradite	WMD87-16 Amphibole	WMD61-7 Amphibole	WMD61-7	WMD87-16	WMD87-16	WMD61-7	WMD61-7
Analysis no.	Spec319-4	Spec327-4	Spec325-6	Spec133-6	Spec314-15-10	Spec-333-15-10	Spec144-2	Spec155-2	Spec318-4	Spec320-4
SiO <sub>2</sub>	51.96	51.13	65.87	69.11	30.91	30.53	37.16	36.63	39.44	39.70
TiO <sub>2</sub>	0.00	0.16	0.00	0.00	38.29	37.32	1.07	0.92	0.69	0.55
Al <sub>2</sub> O <sub>3</sub>	1.35	2.14	19.89	19.43	1.23	1.24	7.79	5.33	12.39	12.37
Cr <sub>2</sub> O <sub>3</sub>	0.00	0.00	0.19	0.00	0.00	0.00	0.00	0.18	0.00	0.00
FeO	12.06	13.42	0.36	0.00	1.08	1.49	17.89	22.7	24.40	23.71
MnO	0.69	0.76	0.00	0.00	0.00	0.00	0.65	0.63	0.62	0.83
MgO	10.19	9.76	0.00	0.00	0.00	0.00	0.00	0.18	6.52	6.31
CaO	23.76	23.72	1.38	0.00	29.45	28.52	34.79	32.93	11.71	11.73
Na <sub>2</sub> O	0.32	0.70	10.67	11.36	0.25	0.00	0.00	0.00	1.60	1.40
K <sub>2</sub> O	0.00	0.00	0.00	0.00	0.00	0.00	0.00	0.00	2.29	2.41
Oxide total	100.33	101.79	98.36	99.90	101.42	99.37	99.35	99.5	99.66	99.01
<i>Structural formula</i>										
Si	1.97	1.91	2.94	3.01	1.99	2.01	2.973	2.962	6.05	6.13
Ti	0.00	0.01	0.00	0.00	1.86	1.84	0.064	0.056	0.08	0.06
Al	0.06	0.09	1.05	1.00	0.09	0.10	0.735	0.508	2.24	2.25
Cr	0.00	0.00	0.01	0.00	0.00	0.00	0	0.012		
Fe <sup>3+</sup>	0.02	0.12	0.00	0.00	0.06	0.08	1.197	1.462	0.57	0.48
Fe <sup>2+</sup>	0.36	0.30	0.01	0.00	0.00	0.00	0.00	0.073	2.56	2.58
Mn	0.02	0.02	0.00	0.00	0.00	0.00	0.044	0.043	0.08	0.11
Mg	0.58	0.54	0.00	0.00	0.00	0.00	0.00	0.022	1.49	1.45
Ca	0.97	0.95	0.07	0.00	2.04	2.01	2.983	2.853	1.93	1.94
Na	0.02	0.05	0.92	0.96	0.03	0.00	0.00	0.00	0.48	0.42
K	0.00	0.00	0.00	0.00	0.00	0.00	0.00	0.00	0.45	0.47
Total cations	4	4	5.00	4.97	6.08	6.05	7.996	7.991	15.924	15.893
Oxygens	6.00	6.00	8.00	8.00	10.00	10.00	12	12	23	23
Mg no.	61.54	64.72	–	–	–	–	–	22.94	36.82	35.96
Wollastonite	50.78	53.07	–	–	–	–	–	–	–	–
Enstatite	30.29	30.37	–	–	–	–	–	–	–	–
Ferrosilite	18.93	16.56	–	–	–	–	–	–	–	–

(continued on next page)



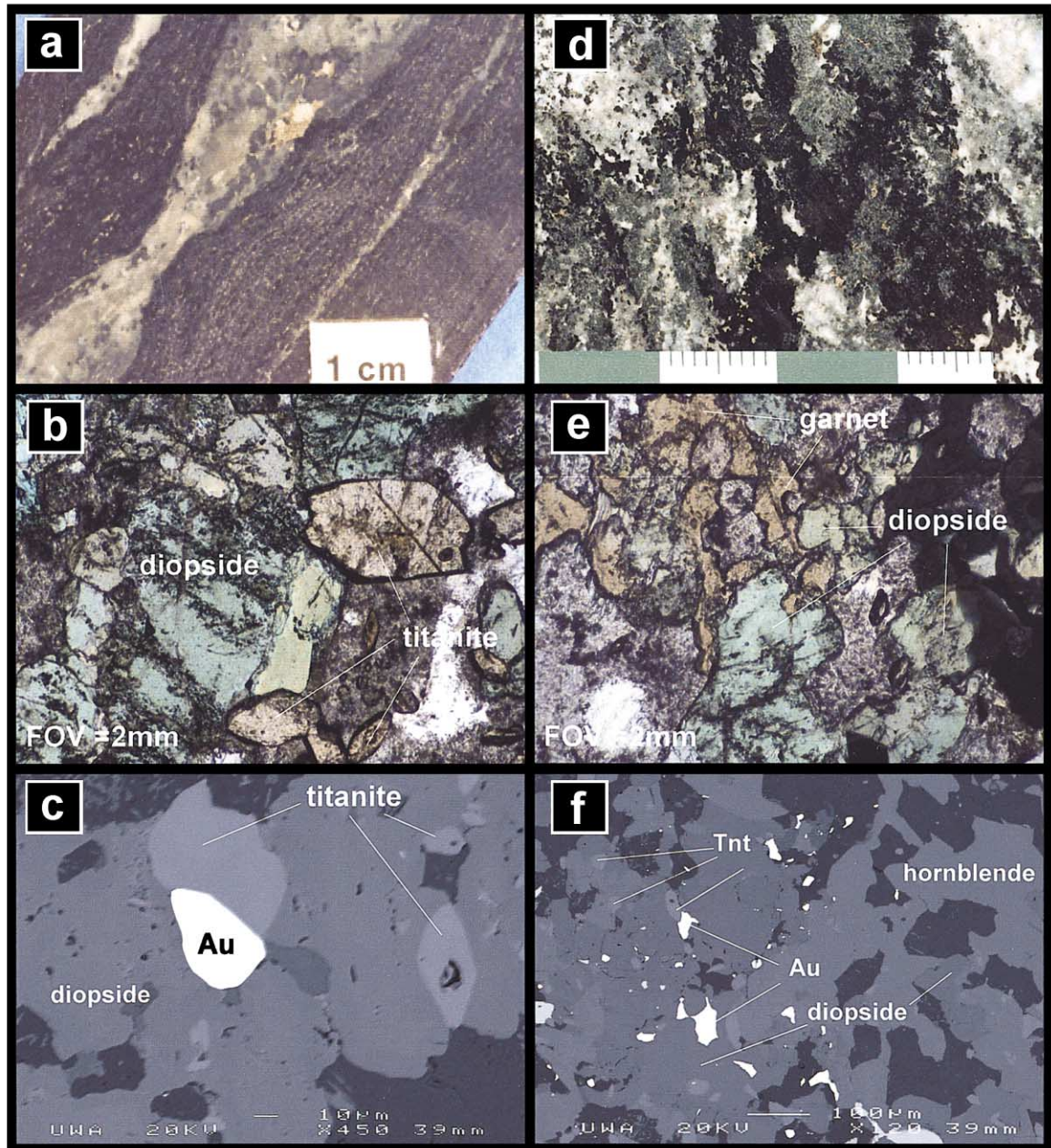
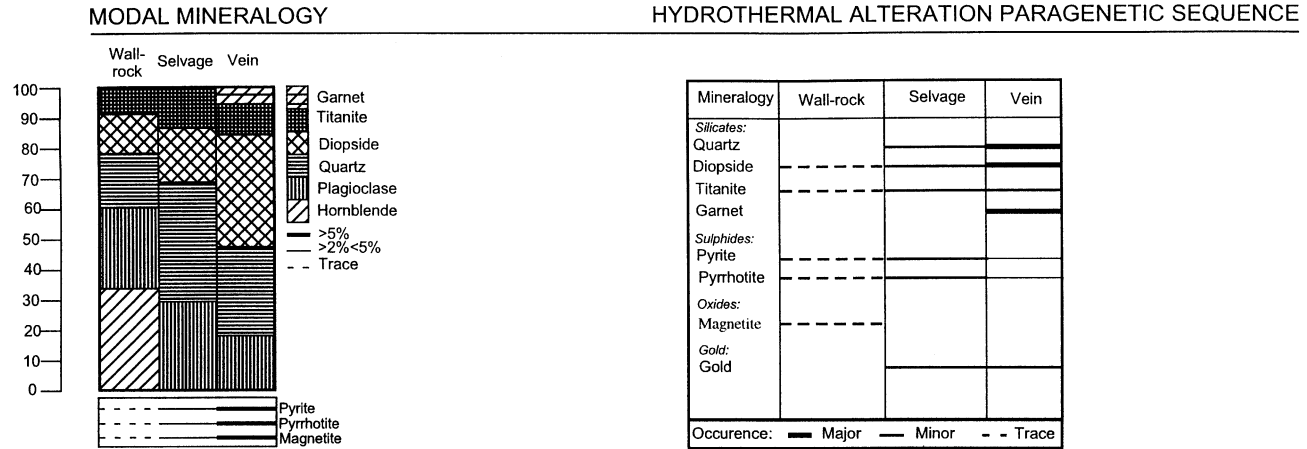


Fig. 7. Main Stage gold mineralisation at the Chalice gold deposit. (a) Type 1 calc-silicate vein. (b) Plane-polarised light photomicrograph of diopside- and titanite-rich core of a Type 1 vein. (c) SEM image displaying the textural relationship between silicate phases and gold in Type 1 veins. (d) Pervasive hydrothermal alteration of mafic amphibolite with diopside and albite replacing magnesio-hornblende and anorthitic feldspar. (e) Plane-polarised light photomicrograph of diopside and garnet which have replaced magnesio-hornblende in mafic amphibolite. (f) SEM image displaying the textural relationship between silicate phases and gold in pervasive hydrothermal alteration of the mafic amphibolite. Note the replacement of magnesio-hornblende with diopside.

Main Stage gold mineralization - Type 1 veins



Main Stage gold mineralization - Pervasive hydrothermal alteration

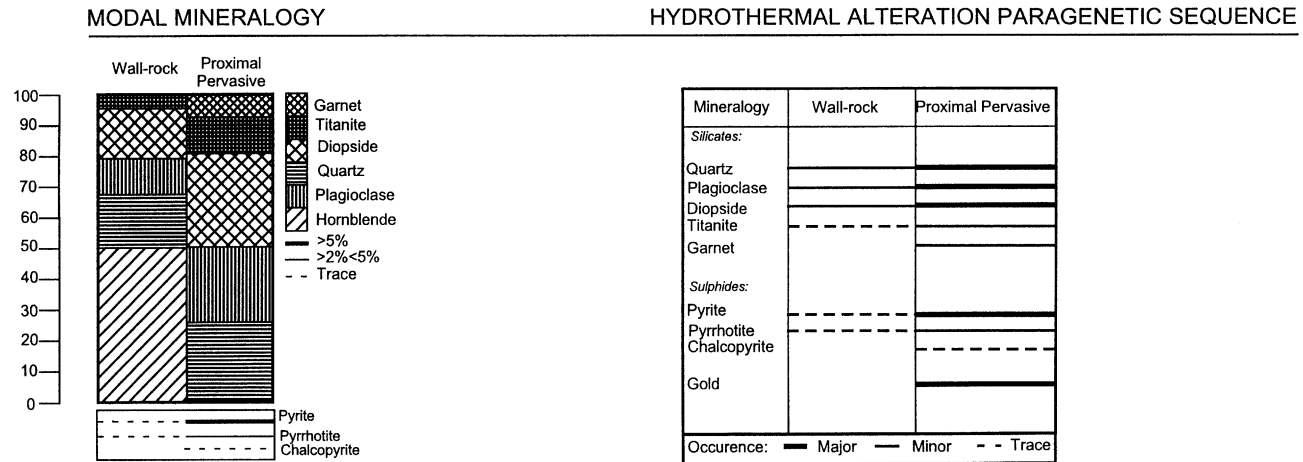


Fig. 8. Modal mineralogy and paragenetic sequence for typical gold-related hydrothermal alteration associated with Main Stage gold mineralisation at the Chalice gold deposit.

to 15% of the vein where present. Type 1 veins are commonly zoned with diopside–garnet-rich cores grading out to quartz–albite–titanite-rich margins. Selvages on veins are typically monomineralic hornblende or quartz–albite–titanite assemblages. Quartz and albite display a pseudo-annealed texture with weak development of triple-point boundaries between the two phases, in most veins. Diopside is commonly coarse-grained ( $\leq 5$  mm) in the core of veins, subhedral to euhedral, and is moderately to strongly poikiloblastic with inclusions of titanite. Diopside grain size decreases ( $\leq 0.8$  mm) towards the margins of veins, and weak subhedral grain development is common in boudinaged veins. Titanite occurs as small ( $\sim 80$ – $100$   $\mu\text{m}$ ) subhedral-to-euhedral grains, commonly as inclusions and intergrown with diopside. Its modal abundance generally increases towards the margins of the veins, and it is a common constituent of vein selvages.

Where developed, garnet occurs as subhedral-to-euhedral grains up to 2 cm in diameter although larger veins display discontinuous aggregates of garnet in the core, which extend for tens of centimeters along strike of the vein. Garnets commonly display anisotropic cores and are complexly zoned with predominantly andradite-rich rims. Compositional variations between alternating zones in the anisotropic cores display a grossular-rich external rim grading into intermediate grossular-andradite compositions. There is also minor development of grossular-almandine.

Accessory sulfide and oxide phases are generally less than 5 modal percent of vein minerals. Pyrrhotite occurs as small ( $\leq 0.8$  mm), subhedral-to-euhedral grains with sporadic exsolution blebs ( $< 0.5$  mm) of chalcocopyrite, in textural equilibrium with silicate phases, commonly intergrown with euhedral pyrite grains ( $\leq 0.8$  mm), and rarely as rims around pyrite. Magnetite occurs as large ( $\leq 2$  mm) pitted subhedral-to-anhedral grains, commonly intergrown with pyrite. Free gold is commonly intergrown, and in textural equilibrium with these prograde phases, particularly diopside, quartz, hornblende, garnet and pyrrhotite (Fig. 7c).

### 5.5. Type 2 veins

Type 2 veins are restricted to the mafic amphibolite, are oriented parallel to the  $S_1$  foliation ( $\sim 70^\circ \rightarrow 261^\circ$ ),

and are less than 5 mm in width. As for Type 1 veins, they are distributed throughout the mafic amphibolite; however, no gold has been detected even on the SEM. Type 2 veins are composed of quartz (30%), strongly sericitised plagioclase (30%; 80% sericite), diopside (20%) and titanite (15%) with accessory pyrrhotite, pyrite and chalcocopyrite. Quartz and plagioclase grains ( $\leq 1$  mm) display very strong sericite alteration. Diopside occurs as small ( $\leq 0.6$  mm) anhedral grains evenly distributed throughout the vein from core to rim and lacks the poikiloblastic texture typical of diopside in Type 1 veins. Titanite is commonly subhedral to euhedral with evenly distributed grains up to 1.5 mm long. The complex intergrowth between sulfide phases, which typifies Type 1 veins, is absent in this vein type. Pyrite occurs as small ( $\leq 0.7$  mm) euhedral grains and commonly contains numerous inclusions of quartz, plagioclase and diopside. Pyrrhotite is less abundant and is generally pitted, subhedral and less than 0.4 mm in width. Chalcocopyrite is only rarely developed, anhedral and generally less than 0.1 mm wide.

### 5.6. Overview of pervasive calc-silicate wall-rock alteration

Pervasive hydrothermal wall-rock alteration is selectively developed in the mafic amphibolite and the calcite–phlogopite–olivine unit at the footwall contact of Dike 2 and constitutes the second most voluminous mineralisation style in Main Stage mineralisation at Chalice (Fig. 7d). Gold-bearing pervasive alteration replaces mafic amphibolite in zones up to 30 m wide and along strike for up to 20 m. Macro- and microscale textural relationships indicate a broadly synchronous timing with respect to Type 1 and Type 2 veins with veins generally cross-cutting pervasive wall-rock alteration and variably being overprinted by pervasive wall-rock alteration. Wall-rock alteration, in general, is characterised by a prograde calc-silicate alteration assemblage of quartz (15%) – feldspar (15%) – diopside (15%) – titanite (10%) – pyrrhotite (10%)  $\pm$  garnet (5%)  $\pm$  hornblende (5%)  $\pm$  biotite (5%)  $\pm$  calcite ( $< 5\%$ )  $\pm$  apatite apatite ( $< 5\%$ )  $\pm$  gold ( $< 3\%$ ) and trace scheelite. Retrograde alteration is expressed as Fe–Mg chlorite (30%), epidote (30%), pyrite (25%), calcite (10%) and unaltered diopside (5%). Deeper extensions of this

alteration style are dominated by a hornblende–calcite assemblage. Common sulfide and oxide phases include pyrrhotite (10%), pyrite (5%), chalcopyrite (<1%) and magnetite ( $\leq 5\%$ ). As for the calc-silicate veins, free gold is locally intergrown with prograde diopside, hornblende and titanite. Rare gold in the retrograde assemblage is common as inclusions in pyrite, associated with strong retrograde epidote–pyrite alteration.

Prograde alteration phases overprint and replace the peak-metamorphic fabric developed in the volcanic units and partly reflect the composition of the host rock. For example, andradite–almandine–grossular garnet and diopside replace mafic amphibolite with komatiite replaced by olivine and phlogopite. Representative modal mineralogy and paragenetic sequence diagrams for gold-related pervasive hydrothermal alteration in the mafic amphibolite are presented in Fig. 8.

### 5.7. Alteration in mafic amphibolite

Pervasive hydrothermal alteration of the mafic amphibolite most commonly involved the replacement of metamorphic magnesio-hornblende by diopside and the replacement of metamorphic magnesio-hornblende and plagioclase by hornblende and albite, respectively (Fig. 7f). There is replacement of the groundmass by quartz and albitic feldspar ( $< \text{An}_{10}$ ), displaying a strong annealed texture, and typically fine-grained ( $\leq 300 \mu\text{m}$ ), in pervasive wall-rock alteration. Diopside occurs as subhedral-to-anhedral grains that normally vary from 0.2 to 0.6 mm, but can be up to 2 cm in diameter. They are generally poikiloblastic with inclusions of quartz, feldspar and titanite, and, where developed, garnet occurs as an intergrown phase (Fig. 7e). Moderate-to-weak subhedral grain development and uralitisation of diopside are typical in sections where retrograde alteration is prevalent. Titanite is generally associated with diopside as subhedral-to-euhedral inclusions and as an intergrown phase, generally  $\leq 0.3$  mm long. It is also widespread as a disseminated phase in the quartz–albite groundmass.

Garnet grains, where developed, are subhedral to euhedral, up to 5 cm in diameter, and are concentrically zoned from rim to core. As for the vein garnets, they are generally poikiloblastic with inclusions of quartz,

feldspar, diopside, titanite and calcite with scheelite as an intergrown phase in some sections. Garnet rims are commonly anisotropic, varying from andradite-rich rims to cores of grossular to grossular-andradite with minor grossular-almandine.

Hornblende is a common phase at depth, but is only moderately developed at shallow levels of the deposit, commonly as subhedral-to-euhedral flame-shaped grains up to 0.8 mm in length, generally randomly oriented in a groundmass of quartz and albite. As for hornblende, biotite is only weakly developed and generally displays strong retrogression to Fe–chlorite. Both calcite and apatite occur in minor to trace abundances with calcite generally restricted to garnet- and biotite-rich zones of wall-rock alteration. Apatite, however, is commonly disseminated throughout all wall-rock alteration. Pyrrhotite is, by far, the most abundant sulfide phase and ranges from subhedral-to-euhedral grains up to 2 cm, but generally 0.6 mm in width. Chalcopyrite exsolution in pyrrhotite is common. Intergrowth with pyrite is also common with rare rims on pyrite of pyrrhotite. Pyrite occurs as euhedral grains ( $< 600 \mu\text{m}$ ) and is generally best developed with retrograde phases such as epidote and Fe–Mg–chlorite. Magnetite and chalcopyrite occur in minor to trace abundances with a strong spatial association to pyrrhotite, commonly with complex intergrowth textures between these three phases.

Free gold (average  $\leq 1$  mm grains) is commonly intergrown with prograde phases such as diopside, hornblende and garnet (Fig. 7f). It also occurs as inclusions in these phases as well as in quartz and albite. Less commonly, there are gold inclusions in pyrite grains associated with strong retrograde epidote–pyrite alteration. This may represent remobilisation of gold in conjunction with Fe release from pyrrhotite to form pyrite during the retrograde path (e.g. Craig and Vokes, 1993).

### 5.8. Alteration in ultramafic rocks

The only ultramafic unit reflecting hydrothermal alteration is the minor calcite–phlogopite–olivine unit at the footwall contact with Dike 2. The protolith for this unit is likely a komatiite, and there are multiple slivers of this rock type, tens of meters off the footwall contact of Dike 2, that display no alteration to the calcite–phlogopite assemblage. This suggests

that this assemblage is hydrothermal in origin and is not the product of prograde-metamorphic reactions. However, gold grades in this hydrothermal assemblage do not exceed 0.01 ppm.

### 5.9. Summary

Main Stage gold mineralisation is collectively defined by gold-bearing Type 1 veins and pervasive wall-rock alteration. It is exclusively developed in the mafic amphibolite and contains up to 95% of the total gold endowment for the entire orebody at Chalice. Although minor hydrothermal alteration is developed in ultramafic rocks at Chalice (calcite–phlogopite–olivine unit), gold enrichment is generally below 0.01 ppm. There are two possible explanations for this. First, veins are preferentially developed in the mafic amphibolite due to a favorable relative competency contrast between it and the ultramafic unit. That is, strain partitioning between the rock types resulted in continued  $S_1$  fabric development in the ultramafic unit and failure in the mafic amphibolite to produce  $S_1$ -parallel Type 1 veins. Second, the whole-rock compositions differ significantly between tholeiitic and komatiitic rocks, as shown by differing alteration assemblages (quartz–albite–diopside–titanite vs. calcite–phlogopite–olivine, respectively). This may have affected selective gold deposition: for example, the higher Fe/Fe+Mg ratio of the tholeiitic rocks would have resulted in destabilisation of reduced sulfur complexes via desulfidation reaction within the fluid due to the deposition of pyrrhotite and/or pyrite (Phillips and Groves, 1983).

## 6. Second Stage gold mineralisation

### 6.1. Introduction

Second Stage gold mineralisation at Chalice is characterised by two styles (Fig. 9): (a) foliation-discordant veins consisting of pyroxene–gold, actinolite–gold and molybdenite–gold veins and (b) disseminated gold in a monzogranite dike. Textural and petrological descriptions of these styles are given below, and representative microprobe analyses of alteration minerals are presented in Table 3.

### 6.2. Analytical methods

Microprobe analysis of Second Stage alteration minerals was conducted at the Centre for Microscopy and Microanalysis at the University of Western Australia. The same instrument and operating conditions used for Main Stage alteration minerals applied.

### 6.3. Overview of foliation-discordant veins

Four types of foliation-discordant veins occur at Chalice (Fig. 10). Each vein type contains gold either intergrown with minerals in the vein, or intergrown with vein selvage minerals. These veins, termed Type 3 through to Type 6, occur exclusively on the hangingwall side of Dike 2, generally within  $\sim 10$  m of the contact, and contribute  $< 3\%$  of the 5% gold endowment for Second Stage mineralisation.

### 6.4. Type 3 veins

Type 3 veins in the mafic amphibolite are commonly moderately folded with axial planes oriented approximately  $60^\circ \rightarrow 270^\circ$ . Symmetry of the veins conforms to that of the  $F_2^1$  folds, and they were likely developed during late  $D_2$ . Type 3 veins are less than 15 mm thick and are primarily composed of quartz (95%) with inclusions of magnesio-hornblende ( $< 5\%$ ) and trace sericite (Fig. 9a). Gold is also a minor constituent ( $< 1\%$ ) of this vein type. Quartz displays strong undulose extinction and moderate subhedral grain development. This suggests a component of dynamic recrystallisation and deformation, as is expected from the folded nature of these veins. Monomineralic magnesio-hornblende selvages accompany veins, and moderate-to-strong subhedral grain development of these amphiboles is common. Gold occurs as inclusions in the vein selvage. There is a distinct lack of sulfides in Type 3 veins; however, gold is a common accessory phase.

### 6.5. Type 4 veins

Type 4 veins are only developed in the mafic amphibolite, are typically 3–5 mm thick and are oriented at  $\sim 20^\circ \rightarrow 085^\circ$ . Type 4 veins are composed of quartz (30%), albite (30%), diopside (25%) and titanite (10%) with accessory ( $< 5\%$ ) pyrrhotite, pyrite, magnetite,

gold and chalcopyrite and trace sericite (Fig. 9b). Type 4 veins are characterised by cores of coarse-grained (<2 mm) subhedral-to-anhedral diopside with inclusions of gold and titanite. Diopside-rich cores grade out into quartz–albite–diopside–titanite-rich rims. Quartz and albite (<0.5 mm) display a pseudo-annealed fabric with moderate development of triple-point junctions between grains. Titanite forms subhedral-to-euhedral grains (<0.2 mm), commonly as inclusions in the quartz–albite groundmass.

The complex intergrowth between sulfide phases characterises Type 4 as well as Type 1 veins. Pyrrhotite, containing small (<0.1 mm) exsolution blebs, occurs as subhedral-to-anhedral grains less than 0.5 mm and commonly contains inclusions of smaller (<0.3 mm) euhedral pyrites. Pyrite is also intergrown with pitted and anhedral magnetite grains (<0.4 mm). Where not intergrown with pyrrhotite, pyrite occurs as euhedral grains with crystal faces up to 0.5 mm wide. Where developed, vein selvages are composed of finer-grained (<0.2 mm) diopside with inclusions of titanite (0.1 mm) in a quartz–plagioclase groundmass. These veins commonly display a “telegraph” texture (Fig. 9b), in which thin (~1 mm), gold–barren quartz–plagioclase–titanite veinlets extend from the veins and preferentially replace the  $S_1$  foliation.

#### 6.6. Type 5 veins

Type 5 veins occur in the mafic amphibolite on the hangingwall side of Dike 2. They are generally up to 3 mm thick, are oriented at  $\sim 60^\circ \rightarrow 085^\circ$ , truncate  $S_1$  and are composed of actinolite (70%), albite (15%) and quartz (15%) with minor titanite, pyrite, magnetite and pyrrhotite (Fig. 9c). Actinolite occurs as coarse (<1 mm) euhedral grains in the core of these veins. Quartz and albite grains (<0.5 mm) constitute the vein rims and are commonly strongly sericite–carbonate altered. Rare titanite occurs as inclusions in, and intergrown with, euhedral actinolite. Pyrite (<0.5

mm) and pyrrhotite (<0.5 mm) occur interstitial to hornblende grains with subhedral-to-anhedral pyrrhotite commonly rimming euhedral pyrite grains. Gold occurs interstitially to, and as inclusions in, actinolite, commonly rims pyrrhotite and magnetite grains and is also common along the cleavage of actinolite grains (Fig. 9d).

#### 6.7. Type 6 veins

Type 6 veins occur both in the mafic amphibolite and the Hangingwall Ultramafic unit; however, this vein type is also best developed in the mafic amphibolite (Fig. 9e). Type 6 veins, oriented at  $\sim 75^\circ \rightarrow 268^\circ$ , are less than 4 mm thick in the volcanic rocks on the hangingwall side of Dike 2 within 10 m of its contact. This vein type is composed of molybdenite (40%), scheelite (30%), magnetite (10%), pyrrhotite (5%) and tellurobismuthite (5%) with accessory pyrite and gold (Fig. 8d). Gold occurs locally as inclusions in pyrrhotite, along the cleavage planes in molybdenite, as inclusions in, and intergrown with, tellurobismuthite, and along fractures in titanite grains.

#### 6.8. Type 7 veins

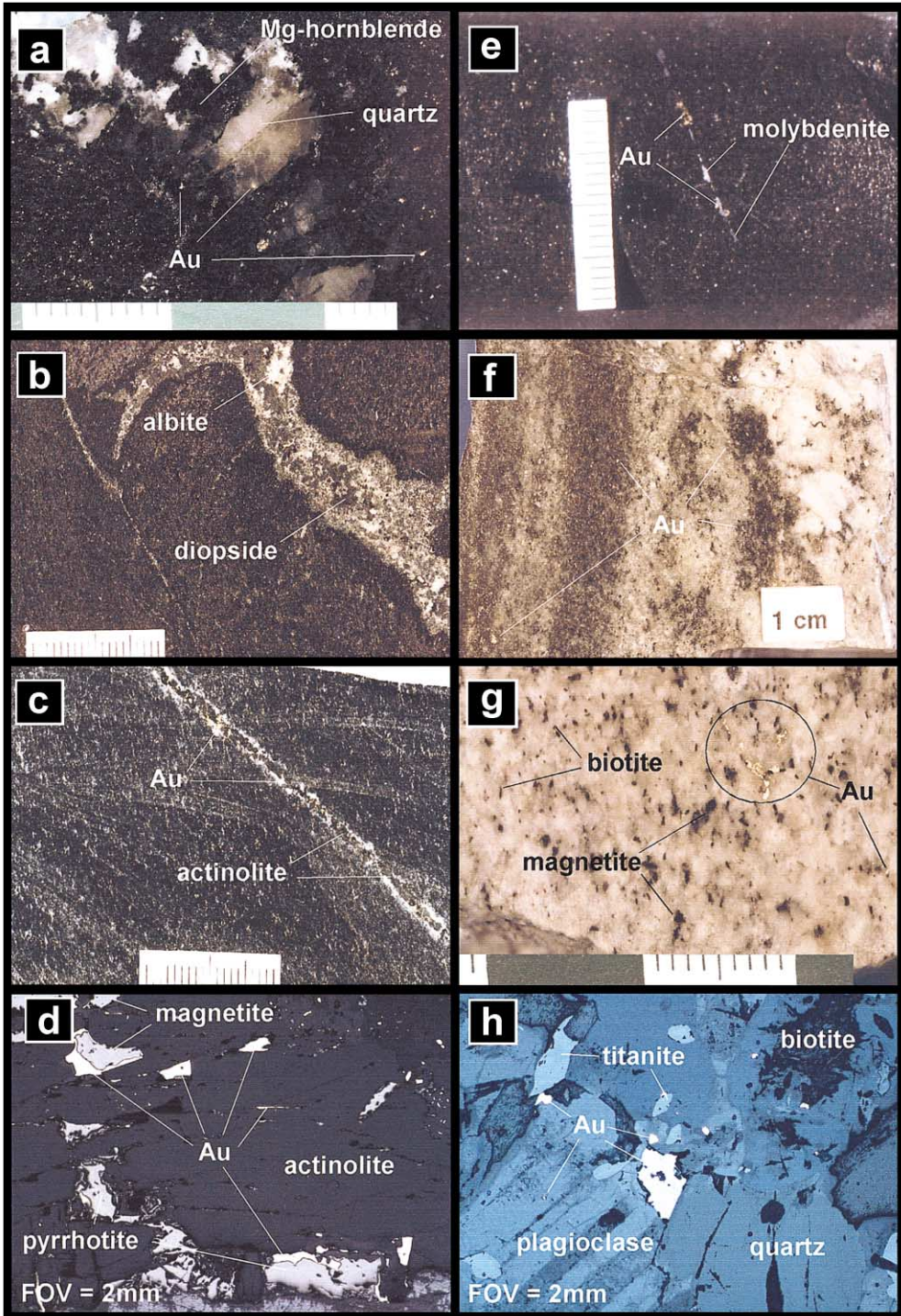
This vein type is characterised by monomineralic quartz tension gash veins. They are nonmineralised and are not further discussed.

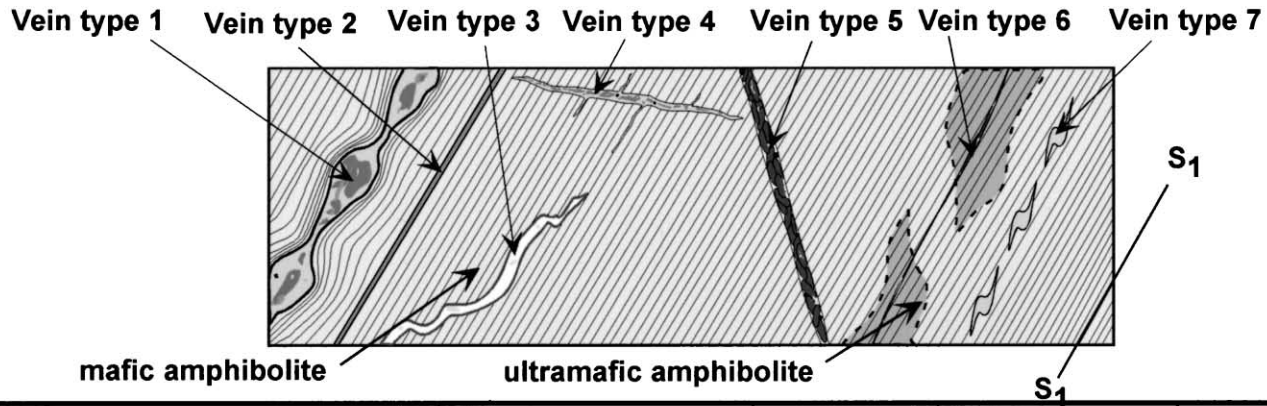
#### 6.9. Disseminated gold mineralisation in Dike 2 monzogranite

Gold mineralisation in the monzogranite dike (Dike 2) is sporadic and varies with respect to its magnitude and distribution throughout the dike. High-grade (up to 20 g/t gold) mineralisation occurs at, and inward (up to 1.5 m) of, the margins of the dike, where it intersects  $S_1$  in the mafic amphibolite. Gold grades decrease towards the center of the dike (0.1–3.0 g/t).

Fig. 9. Second Stage gold mineralisation at the Chalice gold deposit. (a) Type 3 quartz–Au vein. (b) Type 4 quartz–diopside–titanite vein. (c) Type 5 actinolite–Au vein. (d) Reflected light photomicrograph of a Type 5 vein with free gold grown along the cleavage of an actinolite grain. (e) Type 6 molybdenite–Au vein. (f) Altered hangingwall contact of Dike 2 with disseminated free gold. (g) Centre of Dike 2 with disseminated gold in least-altered monzogranite. (h) Photomicrograph of least-altered Dike 2. Image taken with partly crossed polars under simultaneous transmitted and reflected light in order to highlight albite twinning of plagioclase. Note the free gold interstitial to plagioclase and quartz, and as an inclusion in plagioclase.







Vein Type	Vein Mineralogy	Selvedge Mineralogy	Orientation	Siting of Gold	Host Rock
1	Quartz, albite, diopside, titanite, garnet, gold, pyrrhotite, pyrite, magnetite, calcite	Diopside, albite, quartz, titanite	70°→261°	Inclusions in and inter-grown with quartz and diopside	Mafic amphibolite
2	Quartz, albite, diopside	-	70°→261°		Mafic amphibolite
3	Quartz, gold	Magnesian hornblende	~60°→270°	Inclusions in quartz and magnesian hornblende	Mafic amphibolite
4	Quartz, albite, diopside, titanite, gold	Quartz, albite, diopside	~20°→085°	Inclusions in and inter-grown with quartz and diopside	Mafic amphibolite
5	Actinolite, albite, gold, diopside	-	~60°→085°	Inter-grown with actinolite	Mafic amphibolite
6	Molybdenite, gold, tellurobismuthite, scheelite, pyrrhotite, magnetite	-	~75°→268°	Inter-grown with tellurobismutite, molybdenite and pyrrhotite	Mafic and ultramafic amphibolite
7	Quartz	-	80°→270°		Mafic amphibolite

Fig. 10. Schematic diagram of Type 1 to Type 7 veins at the Chalice gold deposit, with main characteristics of each type.

At the dike margins, gold occurs as a disseminated phase, commonly as inclusions in albitised plagioclase, which display moderate-to-strong sericite alteration (Fig. 9f). Plagioclase is also partly replaced by carbonate inward of the dike margin, and biotite is replaced by Fe–Mg chlorite and epidote. Trace coffinite, uraninite, sphalerite and galena are associated with moderate development of chlorite after biotite. Towards the center of the dike, sericite, carbonate, chlorite and epidote alteration intensity decreases (Fig. 9g), and gold occurs as inclusions in plagioclase grains and interstitially at quartz–feldspar grain boundaries (Fig. 9h).

#### 6.10. Summary of Main and Second Stage gold mineralisation

Hydrothermal alteration and associated gold mineralisation at Chalice can be subdivided into Main Stage and Second Stage events, based on cross-cutting relationships in the open pit, underground workings and drillcore. Type 1 veins and gold-bearing pervasive wall-rock alteration are collectively termed Main Stage mineralisation. Second Stage gold mineralisation is defined by foliation-discordant veins and disseminated gold mineralisation in Dike 2. Evidence for two stages of gold mineralisation is as follows.

(1) Gold-bearing foliation-parallel calc-silicate veins (Type 1 veins) and pervasive hydrothermal wall-rock alteration are cross-cut by gold-bearing foliation-discordant veins (Types 3, 4, 5 and 6) and the mineralised Dike 2 monzogranite.

(2) Main Stage mineralisation occurs as stratabound pods, either as veins parallel to the  $S_1$  fabric or foliation-parallel replacive wall-rock alteration. This mineralisation stage is exclusively developed in the mafic amphibolite. Second Stage mineralisation clearly truncates the  $S_1$  fabric at varying angles (see Fig. 10), and is developed in the mafic amphibolite, Hangingwall Ultramafic Unit and monzogranite (Dike 2).

(3) Main Stage gold mineralisation is associated with trace Cu and W, whereas Second Stage gold mineralisation is associated with Bi–Te–Mo–W.

(4) Calc-silicate veins and pervasive wall-rock alteration (Main Stage) display ductile to brittle–ductile deformation textures (boudinage and folding),

whereas Second Stage mineralisation truncates Main Stage mineralisation, is not folded nor boudinaged, and is brittle in nature (excluding the disseminated gold in Dike 2).

#### 6.11. Magmatism and gold mineralisation

Both Main and Second Stage gold mineralisation events are spatially and temporally associated with local monzogranitic dikes (Dikes 1 and 2, Eastern Granite and Basal Pegmatite), and regional granitoids (Woolgangie Super Suite and Pioneer Dome). The monzogranites display similar whole-rock and trace element geochemistry (Table 2; Fig. 3), suggesting that they belong to the same magmatic suite. Relative timing relationships also indicate that there was active felsic magmatism pre-, syn- and post-mineralisation (e.g. Dike 1, Dike 2 and Basal Pegmatite, respectively). However, gold mineralisation in monzogranitic rocks at Chalice is restricted to Dike 1 (<0.2 g/t) and Dike 2 ( $\geq 30$  g/t). These relationships indicate that Main and Second Stage gold mineralisation were temporally bracketed by felsic magmatism, but are more likely to have been related to the evolution of regional magmatism, rather than to a specific intrusion in the local environment.

## 7. Discussion of Main Stage gold mineralisation

### 7.1. Introduction

Many of the general characteristics of Main Stage gold mineralisation at Chalice broadly overlap with those of intrusion-related vein gold, Phanerozoic Au-skarn and Archean hypozonal orogenic lode–gold deposits, located both within the Yilgarn Craton and globally (Tables 5, 6 and 7, and references cited therein). However, numerous differences preclude a direct correlation with any particular deposit type. The following section provides a comparison between the main geological characteristics documented at Chalice (Table 4) and those of intrusion-related vein gold deposits worldwide (Table 5), Phanerozoic Au-skarns and various hypozonal orogenic lode–gold deposits in the Yilgarn Craton (Tables 6 and 7, respectively). For the sake of brevity, these are referred to as

Table 4  
General characteristics of Main and Second Stage gold mineralisation at the Chalice gold deposit

Mineralisation stage	Grade and tonnage (total orebody to June 1999)	Percentage of total orebody	Host rocks	Metamorphic grade	Pluton association	Structural controls
Main Stage	4 Mt@4.9 g/t Au with 589,880 Oz produced	~ 95%	Mafic amphibolite	Amphibolite facies, 490–550 °C, 3–5 kbar		Broad asymmetric folds
Second Stage		~ 5%	Mafic amphibolite, Ultramafic amphibolite and Monzogranite	Amphibolite facies; 490–550 °C; 3–5 kbar	Dike 2 Monzogranite (with disseminated gold)	Veins associated with the intrusion of Dike 2
Timing of gold mineralisation	Wall-rock alteration style	Alteration assemblage/ zonation	Ore minerals	Au fineness	Metal association	Siting of gold
Syn-folding of foliation	Foliation parallel veins and wall-rock replacement	Assemblage: Qtz, ab, dp, tnt, gt, amph, ± bt, ± cct; Vein cores: Dp – gt; Vein selvages: amph, dp	Veins and pervasive: Au, po, py, cpy, mt	Type 1 veins: Avg. 971; Pervasive: Avg. 965	Au, weak Cu	Veins and pervasive alteration: Gold inclusions in dp, qtz, gt, amph; Intergrown and as inclusions in Po
Syn-intrusion of Dike 2	Foliation discordant veins, localised pervasive alteration in monzogranite	Qtz, ab, act, dp, tnt, sch; Vein cores: act, qtz; Vein selvage: Mg-hbl	Veins: Au, moly, TeBi, po, py, mt, cpy; Disseminated: Mt, gn, sp, uran	Au in L. Alt Dike 2: Avg. 751; Au in Alt. Dike 2: Type 5 vein: Avg. 968, Type 6 veins: Avg. 944	Au, Mo, Te, Bi, W, trace Pb–Zn–U	Intergrown with: Act, moly, TeBi, Mg-hbl; Inclusions in: Po, igneous qtz-flid in Dike 2; Interstitial to: Qtz-flid in Dike 2

Abbreviations: L. Alt (least altered).

Key to silicates, carbonates and tungstates: Ab (albite), act (actinolite), amph (amphibole), bt (biotite), cct (calcite), dp (diopside), gt (garnet), hbl (hornblende), Mg-hbl (magnesium-hornblende), qtz (quartz), sch (scheelite), tnt (titanite), uran (uraninite).

Key to ore minerals and oxides: Cpy (chalcopyrite), gn (galena), moly (molybdenite), mt (magnetite) po (pyrrhotite), py (pyrite), sp (sphalerite), TeBi (tellurobismuthite).

intrusion-related, gold-skarn, and orogenic lode–gold deposits, respectively.

### 7.2. Comparison with intrusion-related vein gold deposits

Sillitoe and Thompson (1998) have recognised a suite of five, probably transitional, intrusion-related vein gold deposit groups that they have subdivided based on vein mineralogy and metallogenic associations (see also Lang et al., 2000). Several features of these deposit types, outlined in Table 5, overlap with those of epizonal to mesozonal orogenic gold deposits, leading some authors to suggest that at least some of the deposits within them are, in fact, one and the same (Goldfarb et al., 1997, 1998; Groves et al., 1998). However, when compared to Main Stage gold mineralisation at Chalice, numerous contrasts are evident.

First, metal associations differ significantly with only the Au–Fe oxide–Cu–(Hg) series partially overlapping with that at Chalice. Silicate and oxide vein mineralogy and associated wall-rock alteration also differ with the five series of intrusion-related deposits being collectively dominated by quartz, calcite, muscovite, wolframite, specular hematite, magnetite and chlorite after biotite (high *T*) vein assemblages and sericite, muscovite, quartz, K-feldspar, biotite and albite wall-rock alteration assemblages. Veins and wall-rock alteration associated with Main Stage gold mineralisation at Chalice are characterised by calc-silicate alteration phases, dominated by quartz, albite, diopside, titanite and garnet as well as minor magnetite. Structural style and tectonic setting are also different. The intrusion-related deposits are located typically in the upper 7 km of the crust in a brittle to brittle–ductile structural régime, generally inboard of the collisional suture in arc to backarc settings (Sillitoe and Thompson, 1998; Lang et al., 2000). However, hypozonal orogenic gold deposits form below 12-km depth in dominantly ductile settings, within deformed accretionary belts adjacent to continental magmatic arcs (Groves et al., 1998).

The aforementioned differences indicate a strong disassociation between Main Stage gold mineralisation at Chalice and the intrusion-related suite of deposits as defined. The spatial association with granitic rocks is the only common attribute.

### 7.3. Comparison with Phanerozoic gold-skarn deposits worldwide

There has been much debate in the literature with respect to whether Archean hypozonal orogenic lode–gold deposits are ancient analogues of Phanerozoic gold-skarns (e.g. Mueller, 1991, 1997; Mueller and Groves, 1991; Hagemann et al., 2000). Skarn is defined by Einaudi et al. (1981) as “coarse grained Ca–Fe–Mg–Mn silicates formed by either metamorphic recrystallisation, bimetasomatic reactions between unlike lithologies or infiltration metasomatism involving hydrothermal fluids of magmatic origin”. Meinert (1998) went further to suggest that “skarns are a simple rock type defined by its mineralogy and dominated by calc-silicate minerals such as calcic-garnet and pyroxene. . .and can form in almost any rock type including limestone, shale, granite, iron formation, basalt and komatiite”. Effectively, in both cases, the term “skarn” is a mineralogical classification with calcic-garnet- and pyroxene-constituting essential phases. Törnebohm (1875) was the first to publish the term “skarn” based on work in the Persberg area, Sweden. This type locality has skarn formed in felsic metavolcanic rocks and iron formation, not directly associated with a pluton or limestone. However, because the majority of gold-skarns described in the literature contain a proximal causative pluton, generally associated with calcareous rocks (see reviews by Einaudi, 1981; Meinert, 1998; Ray and Dawson, 1998), the notion that skarns are the product of metasomatism by magmatic fluids is prevalent. The general characteristics of gold-skarns based on the literature (Table 6) are compared with Main Stage gold mineralisation at Chalice (Table 4), and it is apparent that they differ significantly. Examples as follows.

(1) Phanerozoic gold-skarns are commonly located in either very low-grade metamorphic, or unmetamorphosed, calcareous sedimentary host rocks. Host rocks at Chalice were at mid-amphibolite facies-metamorphic grade at the time of mineralisation.

(2) Hornblende–feldspar geobarometry at Chalice indicates crustal depths of 12–14 km, whereas the characteristic depth for the majority of Phanerozoic gold-skarns is between 2 and 5 km.

(3) Main Stage gold mineralisation at Chalice is primarily structurally controlled, whereas gold mine-

Table 5  
 General characteristics of selected intrusion-related vein gold deposits worldwide  
 Compiled from Sillitoe and Thompson (1998), Thompson et al. (1999) and Lang et al. (2000).

Major metal association classes	Deposit example	Deposit for comparison	Size	Country rocks	Pluton association
Au–Fe oxide–Cu–(Hg)	Mantos de Punitaqui (Chile)	Mantos de Punitaqui	~ 2 Mt@4 g/t Au produced	Volcano-sedimentary rocks	Monzodiorite
Au–Cu–Mo–Zn	Snip (Canada) Salave (Spain)	Snip	1.27 Mt@27 g/t Au produced	Sedimentary rocks	Quartz monzodiorite porphyry
Au–As–Pb–Zn–Cu–Ag	Parcoy-Pataz (Peru) Kori Kollo (Bolivia) Charters Towers (Australia) Linglong (China)	Parcoy-Pataz	~ 8 t/year Au produced	Monzodiorite to granodiorite	Monzodiorite to granodiorite
Au–Te–Pb–Zn–Cu	Dongping (China) Kidston (Australia)	Dongping	>16 Mt@6 g/t Au	Syenite and alkali–feldspar syenite	Syenite–monzonite
Au–As–Bi–Sb	Ryan Lode (Canada) Fort Knox (Alaska)	Ryan Lode	26 t Au	Granite porphyry and volcano-sedimentary rocks	Granodiorite, granite

Key to silicates and carbonates: Ab (albite), bt (biotite), cct (calcite), chl (chlorite), K-feld (K-feldspar), musc (muscovite), qtz (quartz), ser (sericite).

Key to ore minerals and oxides: Asp (arsenopyrite), boul (boulangerite), cpy (chalcopyrite), gn (galena), mt (magnetite), moly (molybdenite), po (pyrrhotite), py (pyrite), schw (schwartzite), spec hm (specular hematite), sp (sphalerite), sb (stibnite), tel (tellurides), wf (wolframite).

Structural controls	Wall-rock alteration	Zoning	Ore minerals	Siting of gold	<i>P-T</i> conditions of mineralisation
Regional sinistral strike-slip fault system	Vein: qtz, cct; Wall-rock: ser	Sericite alteration halos to veins	Spec hm, mt, cpy, py, schw	Associated with spec hm and cpy	206–255 °C; <2 kbar
Brittle-ductile shear zone	Vein: chl, bt, cct, qtz; Wall-rock: bt, K-feld, cct, qtz, ser	Wall-rock inner: bt; Wall-rock outer: K-feld, cct, qtz, ser	Po, py, moly, sp		
Regional west-verging thrust faults	Stg 1 vein: musc, py, asp, wf; Stg 2 vein: py, sp, gn, cpy; Wall-rock: qtz, musc, py	Qtz-musc-py alteration halos to veins	Py, asp, wf, sp, gn, cpy	Associated with py, asp, wf, sp, gn and cpy	130–328 °C; <2 kbar
Regional fault	Vein: qtz, K-feld; Wall-rock: K-feld	K-feld alteration halos to veins	Py, spec hm, tel, gn, sp, cpy		240–350 °C; 500–690 bars
Local shear veins and stockwork veins	Shear veins: qtz, ser; Stockwork veins: qtz, ab, cct	Sericite alteration halos to veins	Asp, sb, sp, sch, cpy, moly, boul, Pb-Bi sulphosalts	Strong Au-Bi association	280–350 °C; <1 kbar

Table 6  
General characteristics of selected Phanerozoic gold-skarns worldwide

Deposit	Grade and tonnage	Country rocks	Pluton association	Structural controls	Wall-rock alteration
Big Gossan, Irian Jaya	37.4 Mt@2.69%Cu 1.02 g/t Au 16 g/t Ag	Dolomite, dolomitic limestone, siltstone, sandstone	Granodiorite	Imbricate thrust sheets and isoclinal folds	Prograde: gross, dp; Retrograde: amph, chl, ep
McCoy, Nevada	15.6 Mt@1.4 g/t Au	Carbonate and siliceous sedimentary rocks	Quartz monzonite to granodiorite	Regional shearing	Endoskarn: K-feld, ep, act, gt, dp; Exoskarn: gt, dp, cct, K-feld, chl K-feld, bt
Copper Canyon, Nevada	10 Mt@0.8 g/t Au 0.8%Cu	Limestone	Granodiorite	Shear zone	Prograde: gt, pyx; Retrograde: woll, preh, ep, chl
Nickel Plate, Hedley District, BC, Canada	13.4 Mt@5.3 g/t Au	Calcareous and tuffaceous siltstones and limestones	Diorite to gabbro	Shearing	Prograde: pyx, gt; Retrograde: cct, qtz, ep, amph
Buckhorn, Washington	7.3 Mt@4.6 g/t Au	Clastic and carbonate sedimentary rocks, andesitic flows	Diorite to granodiorite	Associated shearing	Prograde: pyx, gt; Retrograde: cct, qtz, ep, amph
Mason Valley, Yerington District, Nevada	1.5 Mt@2.7 wt.% Cu	Limestone	Granodiorite to quartz monzonite	Strong regional folding and faulting	Gt, pyx, trem, mt, tc, cct

Key to silicates, carbonates and tungstates: Act (actinolite), amph (amphibole), andr (andradite), bt (biotite), cct (calcite), chl (chlorite), dp (diopside), ep (epidote), gross (grossular), gt (garnet), K-feld (K-feldspar), preh (prehnite), pyx (pyroxene), qtz (quartz), tc (talc), trem (tremolite).

Key to ore minerals and oxides: Asp (arsenopyrite), cc (chalcocite), cpy (chalcopyrite), elec (electrum), gn (galena), loel (loellingite), mar (marcasite), po (pyrrhotite), py (pyrite), sp (sphalerite).



Zoning	Ore minerals	Siting of gold	Metal association	<i>P-T</i> conditions of mineralisation	References
Proximal: gross, dp; Intremediate: gross–andr, dp–hed; Distal: andr, hed	Py, po, cpy, elec, sp, gn	Cu and Au in cpy	Cu, Au, Ag	369–460 °C < 1.5 kbar	Meinert et al. (1997)
Proximal: gt, dp; Distal: bt, amph, chl, cct, K-feld	Py, po, cc, cpy, sp	Free Au	Au, Ag, Cu	330–590 °C ~ 350 bars	Kuyper (1988)
Proximal: gt, pyx; Intermediate: bt, K-feld, pyx; Distal: bt, amph (Meinert, 1998)	Py, cpy, po, mar Asp, loel, po (Meinert, 1998)	K-feld, bt Au with gt and pyx	Au, Cu Au	375°C < 1 kbar 460–480 °C	Kotlyar et al. (1988) Ettlinger et al. (1992)
Proximal: gt, mt; Intermediate: gt, pyx, ep; Distal: pyx, amph	Cpy, py, po	Au with Bi metals in late stage fractures in prograde minerals. Associated with po in mt zones	Au, Cu	360–465 °C < 2 kbar	Hickey (1992)
Proximal: gt, pyx, mt; Distal: trem, cct, tc, dol	Cpy, py	Cpy interstitial to gt and pyx zones	Cu	~ 600 bar	Einaudi (1977)

Table 7  
General characteristics of selected Archean hypozonal orogenic lode–gold deposits of the Yilgarn Craton, Western Australia

Region in the Yilgarn Craton	Deposit	Grade and tonnage (to Dec 88)	Host rocks	Metamorphic grade	Structural controls	Timing of Au mineralisation
SCP	Marvel Loch	2.2 Mt@3.5 g/t Au	Pillowed meta-komatiites and gabbros	Amphibolite facies; >550 °C	Broad ductile shear zones with penetrative foliation	Post-peak-metamorphism
SCP	Nevoria	1.86@3.5 g/t Au	Grun–qtz BIF, minor u/m and mafic amphibolites	Amphibolite facies; 570–610 °C	Narrow ductile shear zone	Post-peak-metamorphism
SCP	Frasers	0.87 Mt@10.9 g/t Au	Ultramafic rocks	Mid-amphibolite facies	Ductile shear zone	Syn-shear zone development and peak-metamorphism
SCP	Hopes Hill	32,500 kg Au	Meta-basalt, meta-komatiite, meta-sedimentary rocks	Mid-amphibolite facies	Ductile shear zones	Syn- to post-peak-metamorphism
SCP	Transvaal	87,729 t@6.82 g/t Au (production 1996–1997)	Meta-pelite, meta-komatiite	Mid-amphibolite facies; ~ 550 °C; 2–4 kbar	Ductile shearing along lithological contacts	Syn-peak-metamorphism
CG	Kings Cross	216,415 t@5.08 g/t Au (April 1991)	Meta-basalt	Lower-amphibolite facies	Brittle–ductile shear zones	Syn-peak-metamorphism
CG	Tindals Group	~ 1 Mt@4.74 g/t Au (May 1993)	Porphyry and dolerite in meta-komatiite	Mid-amphibolite facies	Shear zones at lithological contacts	Syn-peak-metamorphism
CG	Burbanks Group	0.5 Mt@20.12 g/t Au (December 1989)	Meta-basalt	Mid-amphibolite facies	Brittle–ductile shear zones	Syn-peak-metamorphism
NR	Mararoa-Crown	6.9 Mt@10.4 g/t Au (June 1987)	Meta-basalt	Lower-amphibolite facies	Brittle–ductile shear zones	Syn- to post-peak-metamorphism
NR	Scotia	677,000 t@6 g/t Au (June 1987)	Meta-basalt, meta-komatiitic basalt	Mid-amphibolite facies; ~ 560–670 °C; 2–4 kbar	Ductile shear zone	Syn-peak-metamorphism

Abbreviations: SCP= Southern Cross Province; CG= Coolgardie Goldfields; NR= Norseman Region.

Key to silicates, carbonates and tungstates: Ab (albite), act (actinolite), alm (almandine), amph (amphibole), bt (biotite), cct (calcite), chl (chlorite), clz (clinozoisite), cord (cordierite), cum (cummingtonite), dp (diopside), gt (garnet), hbl (hornblende), hed (hedenburgite), K-feld (K-feldspar), Mg-hbl (magnesium-hornblende), ol (olivine), phlog (phlogopite), plag (plagioclase), qtz (quartz), sch (scheelite), tnt (titanite), trem (tremolite), uran (uraninite).

Key to ore minerals and oxides: Asp (arsenopyrite), Cpy (chalcopyrite), gn (galena), ilm (ilmenite), loel (loellingite), lx (leucoxene), mar (marcasite), moly (molybdenite), mt (magnetite), pent (pentlandite), po (pyrrhotite), py (pyrite), sp (sphalerite), TeBi (tellurobismuthite).

Wall-rock alteration style	Alteration assemblage/zonation	Ore minerals	Siting of gold	Metal association	<i>P-T</i> conditions of mineralisation	References
Foliation parallel tabular zones, predominantly in meta-komatiite	Inner: ol, cct; Int.: dp, amph, phlog, locally qtz-dp veins; Outer: trem, chl	Po, py, asp, loel, cpy, gn, sp	Free gold	Au, Ag, As, Sb, Pb, W	Max <i>T</i> = 620 °C; 4 ± 1 kbar	Mueller (1991)
Massive and vein controlled replacement in grun-qtz BIF	Inner: hed, minor alm; Outer: Fe act and hbl	Po, cpy, asp, loel, py	Free gold	Au	550–580 °C; 4 ± 1 kbar	Mueller (1997)
Qtz-dp-calc veins with 10 mm wide alteration halos	Inner: layers of dp and amph; Int.: bt, plag layers; Outer: bt, cord, cum layers	Po, cpy, pent, gn	Gold inclusions in sulfides and quartz. Associated with Po in siliceous wall-rocks	Au, Fe, Cu	555 ± 35 °C; 3 kbar	Barnicoat (1989)
Folded and boudinaged qtz-plag-dp-cct-tnt veins	Inner: qtz, bt, dp, amph, plag, gt, K-feld; Outer: bt, amph, plag	Po, py, cpy	Free gold	Au, Ag	500–700 °C	Ridley et al. (1995); Bloem et al. (1994)
Qtz-sulpharsenide veins	Inner: qtz, bt, dp, amph, plag, gt, K-feld; Outer: bt, amph, plag	Po, loel, asp, electrum	Electrum in loel and loel-po contacts. Gold in po	Au, As	500–700 °C	Dalstra et al. (1998)
Laminated quartz reefs	Inner: amph, bt, cct, plag, qtz, tnt, K-feld, Mg-chl	Po, aps, sp, cpy, py, gn	Intergrown with sulfide phases	Au	3–4 kbar (Groves et al., 1975)	Knight et al. (1993), Groves et al. (1975), Ridley et al. (2000)
Veinlets along lithological contacts and associated intense wall-rock alteration	Inner: hbl, plag, cct, qtz, chl, bt, gt	Po, sp, cpy, py, sch, ilm	Free gold in altered wall-rock and veinlets	Au	495–596 °C (avg. 542 ± 25 °C); 4.3–5.1 ± 0.3 kbar	Knight et al. (1993), Ridley et al. (2000)
Laminated quartz reefs	Inner: gt, bt, hbl, qtz, cct, plag	Po, py, sp, gn, asp, sch, rut	Intergrown with sulfide phases	Au	400–500 °C; 3–4 kbar (Groves et al., 1975)	Knight et al. (1993), Groves et al. (1975), Ridley et al. (2000)
Laminated quartz reefs	Inner: act, bt, qtz, plag, cct, lx, tnt, sch; Outer: hbl, act, bt, qtz, plag, cct, ilm	Py, gn, tel, Au, po, sp, cpy, mar	Gold in fractures in euhedral pyrite, and at quartz grain boundaries	Au	470–500 °C; 3 kbar	McCuaig et al. (1993), Ridley et al. (2000)
Shear hosted veinlets and associated wall-rock	Inner: act, qtz, cct, dp, clz, plag; Outer: hbl, bt, plag, ilm, qtz	Po, py, cpy, asp, bi, Au	Inclusions in quartz	Au	>500 °C; 3–5 kbar	McCuaig et al. (1993), Ridley et al. (2000)

realisation in gold-skarns is controlled by metasomatic replacement commonly involving magmatic fluids.

(4) Mineralisation in gold-skarns is generally associated with a proximal contemporaneous pluton. In contrast, Main Stage gold mineralisation at Chalice is cross-cut by proximal monzogranites, which indicates that it predated local felsic magmatism in timing.

(5) Phanerozoic gold-skarns are characterised by prograde anhydrous alteration assemblages (including calcic-garnet + pyroxene), whereas Main Stage gold mineralisation at Chalice exhibits hydrous phases (amphibole and biotite) as part of the prograde alteration assemblage.

In summary, from a mineralogical viewpoint, Main Stage gold mineralisation may tentatively be classified as skarn, as has been proposed by Mueller (1991, 1997) for other hypozonal orogenic lode–gold deposits in the Yilgarn. However, with respect to genetic characteristics, such as structural controls, alteration systematics and zoning, pluton association and crustal depth of formation, the application of the term skarn to define Main Stage gold mineralisation at Chalice is equivocal.

#### 7.4. Comparison with hypozonal orogenic lode–gold deposits of the Yilgarn Craton

Archean hypozonal orogenic lode–gold deposits are defined as “(gold-bearing) vein systems with a unique spatial and temporal association with orogeny, that form at depths below 12 km and at temperatures exceeding 475 °C”, according to the classification of Groves et al. (1998). These deposits also commonly display extensive wall-rock replacement associated with gold mineralisation. The general characteristics of Main Stage gold mineralisation at Chalice are outlined in Table 4 and are compared with those of typical orogenic lode–gold deposits in the three main high-temperature settings of the Yilgarn Craton (Table 7). Similarities include:

1. Grade and tonnage: Generally small (< 1 Moz) high-grade (5–10 g/t Au) orebodies.
2. Host-rock composition and metamorphic grade, dominated by metabasalts metamorphosed to mid- to upper-amphibolite facies grade ( $\sim 550 \pm 50$  °C and  $\sim 2$ – $5$  kbar) and corresponding to crustal depths > 12 km.

3. Wall-rock alteration assemblages associated with gold mineralisation, dominated by a quartz + diopside  $\pm$  calcic-amphibole  $\pm$  garnet  $\pm$  calcite  $\pm$  titanite assemblage.
4. Siting of gold: Commonly as inclusions and intergrown with pro-grade calc-silicate phases (e.g. diopside and garnet) and associated with sulphides such as pyrrhotite.

The main differences between Main Stage gold mineralisation at Chalice and Yilgarn orogenic lode–gold deposits in higher-temperature settings are the structural controls on mineralisation. Hypozonal orogenic lode–gold deposits are typically hosted in either discrete ductile shear zones displaying penetrative shear fabrics, or brittle–ductile shear zones and associated laminated quartz reefs. This contrasts with Main Stage gold mineralisation at Chalice, which is controlled by local, broad asymmetric folds, lacking penetrative shear fabrics.

Collectively, the general characteristics of Main Stage gold mineralisation at Chalice are equivalent to hypozonal orogenic lode–gold mineralisation documented elsewhere in higher-temperature greenstone terranes of the Yilgarn Craton. The differences simply reflect a variation on the typical structural controls in this deposit type.

## 8. Discussion of Second Stage gold mineralisation

Second Stage gold mineralisation is temporally bracketed between the Main Stage event and the intrusion of the Basal Pegmatite. As Main Stage gold mineralisation is controlled by D<sub>2</sub> folds, the Second Stage event is effectively constrained by magmatic events. Gold in this event is associated with Bi–Te–Mo–W trace Zn–Pb and U (Table 4) and occurs in discrete veins and as a disseminated phase in monzogranite Dike 2 (Fig. 9). These features contrast with those of the Main Stage event (Table 4; Fig. 7) and are atypical of hypozonal orogenic lode–gold deposits elsewhere in the Yilgarn Craton (Table 7). Based on the metal association as well as the spatial and temporal relationship with felsic magmatic intrusions, Second Stage mineralisation reflects a closer affinity to intrusion-related gold systems, in particular, those in the Tombstone Plutonic Suite, Yukon (see Lang et

al., 2000; Table 5). Textures, such as gold interstitial to, and as inclusions in, quartz and plagioclase of the least-altered Dike 2 monzogranite (Fig. 9h), suggest an inherent relationship between monzogranite crystallisation and gold precipitation, although gold-bearing miarolitic cavities, which are common in many Tombstone Plutonic Suite intrusions (Duncan et al., 1997), are absent. The fact that Dike 2 is mostly mineralised (99%) where it intersects Main Stage gold mineralisation suggests that Second Stage gold may have been remobilised from the Main Stage although the specific element association of Au–Bi–Mo–Te–W is more indicative of a separate gold mineralising event. Thus, as the characteristics of Second Stage mineralisation overlap with both epi- to mesozonal orogenic lode–gold and intrusion-related deposits, classification of Second Stage mineralisation is equivocal, at our current level of understanding of the deposit.

Therefore, bearing in mind that both Main and Second Stage gold mineralisation are temporally bracketed by magmatism and that only the minor Second Stage event is potentially intimately associated with magmatism, it is more appropriate at the current level of understanding to consider gold mineralisation as an event associated with the broader evolution of a magmatic/metamorphic system in the later stages of orogenesis. It is currently uncertain as to whether the intrusion of Dike 2 contributed magmatic-gold to the overall budget of the deposit or if gold was assimilated and remobilised from the Main Stage event. This problem will be addressed during on-going research.

## 9. Descriptive model

### 9.1. Introduction

The geological characteristics and relative timing between metamorphism, deformation, magmatism and hydrothermal alteration at Chalice can be synthesised to produce a depositional model for Main and Second Stage gold mineralisation. This model excludes genetic connotation with respect to the fluid source for metals. A series of schematic diagrams, which represent the sequential evolution of the Chalice gold deposit, are presented in Fig. 11 and summarised in

Fig. 12. Deformation events discussed in the following section relate to local events recognised at Chalice and not the regional deformation events used in reference to the Kalgoorlie Terrane (e.g. Hammond and Nisbet, 1992; Myers, 1993, 1997; Williams and Whitaker, 1993; Archibald, 1998).

### 9.2. Evolution of the Chalice gold deposit

#### 9.2.1. Predeformation

The earliest event at Chalice corresponds to the regional eruption of the mafic–ultramafic and felsic volcanic rocks of the Kalgoorlie Terrane, which occurred from 2700–2690 Ma for the mafic–ultramafic unit to ~2680 Ma for the felsic volcanic unit (Claué-Long et al., 1988; Nelson, 1995). Krapez et al. (2000) suggest ages as young as ~2660 Ma for felsic detritus in overlying sedimentary sequences.

#### 9.2.2. $D_1$ to $D_2$

The  $D_1$  event and peak metamorphism were broadly synchronous. Ages for peak-amphibolite facies-metamorphic conditions in the Norseman–Wiluna greenstone belt are equivocal. Nelson (1997) interprets a ca. 2630 Ma timing for peak-metamorphism although regional high-grade metamorphism is also interpreted to have occurred at ca. 2660 to 2640 Ma (Swager, 1997). For the purpose of this relative timing discussion, it is sufficient to recognise that the volcanic sequence was deposited (Fig. 11a) and subsequently deformed during peak-metamorphic conditions ( $D_1$ ) to produce a deposit-scale foliation,  $S_1$  (Fig. 11b).

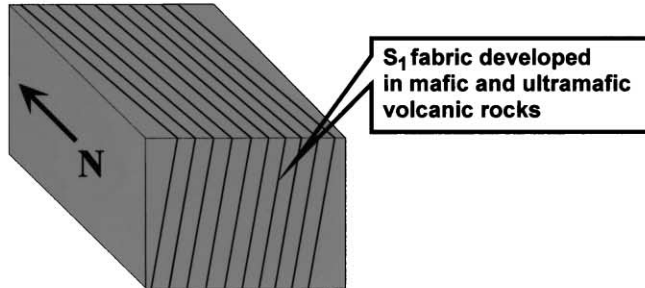
Magmatism in the local mine environment (Fig. 11c) produced the Dike 1 monzogranite, which variably truncates the  $S_1$  fabric, and is subsequently calc-silicate altered. The  $D_2$  event involved folding ( $F_2^1$ ) of the  $S_1$  fabric and development of  $S_1$ -parallel gold-bearing Type 1 calc-silicate veins and pervasive wall-rock alteration. The orebody occurs as a broadly stratabound body, approximately  $45 \times 170 \times 300$  m in dimensions (Fig. 11d). This represents the Main Stage gold mineralisation event, and accounts for up 95% of the gold endowment at Chalice.

#### 9.2.3. Late $D_2$ to $D_4$

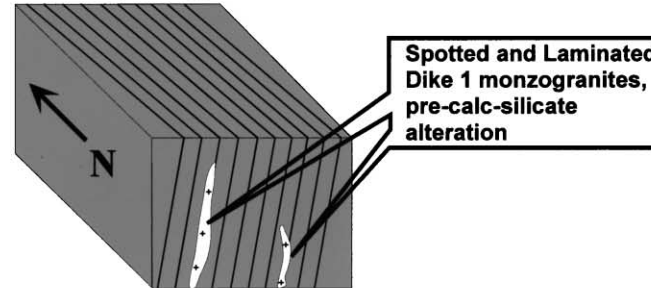
The Dike 2 monzogranite cross-cuts the  $S_1$  fabric and  $F_2^1$  folds late in the evolution of the  $D_2$  event. The

(a) **Pre-deformation: Mafic and ultramafic volcanism and deposition of greenstone sequence**

(b) **D<sub>1</sub>**



(c) **Late D<sub>1</sub> magmatism**



(d) **D<sub>2</sub>**

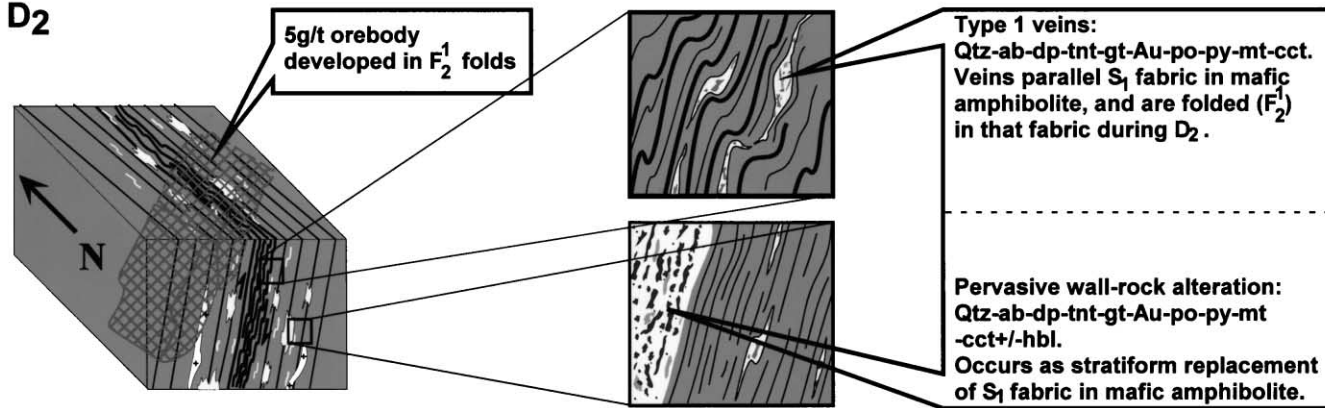


Fig. 11. Evolution of the Chalice gold deposit. See text for discussion. Abbreviations: ab = albite, bt = biotite, cct = calcite, dp = diopside, fld = feldspar, gt = garnet, hbl = hornblende, mt = magnetite, ol = olivine, phl = phlogopite, plag = plagioclase, po = pyrrhotite, py = pyrite, qtz = quartz, tnt = titanite, trem = tremolite.

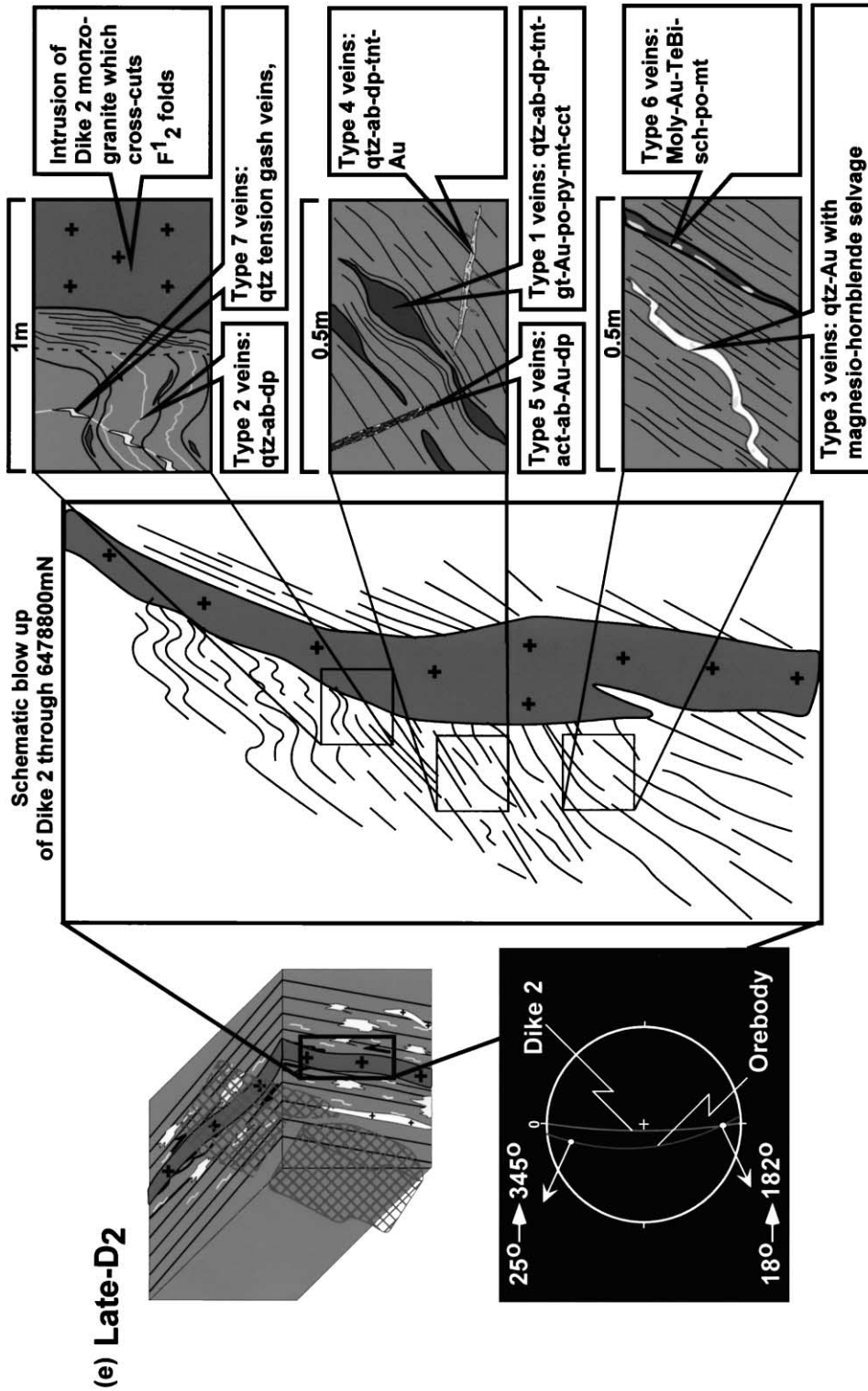


Fig. 11 (continued).

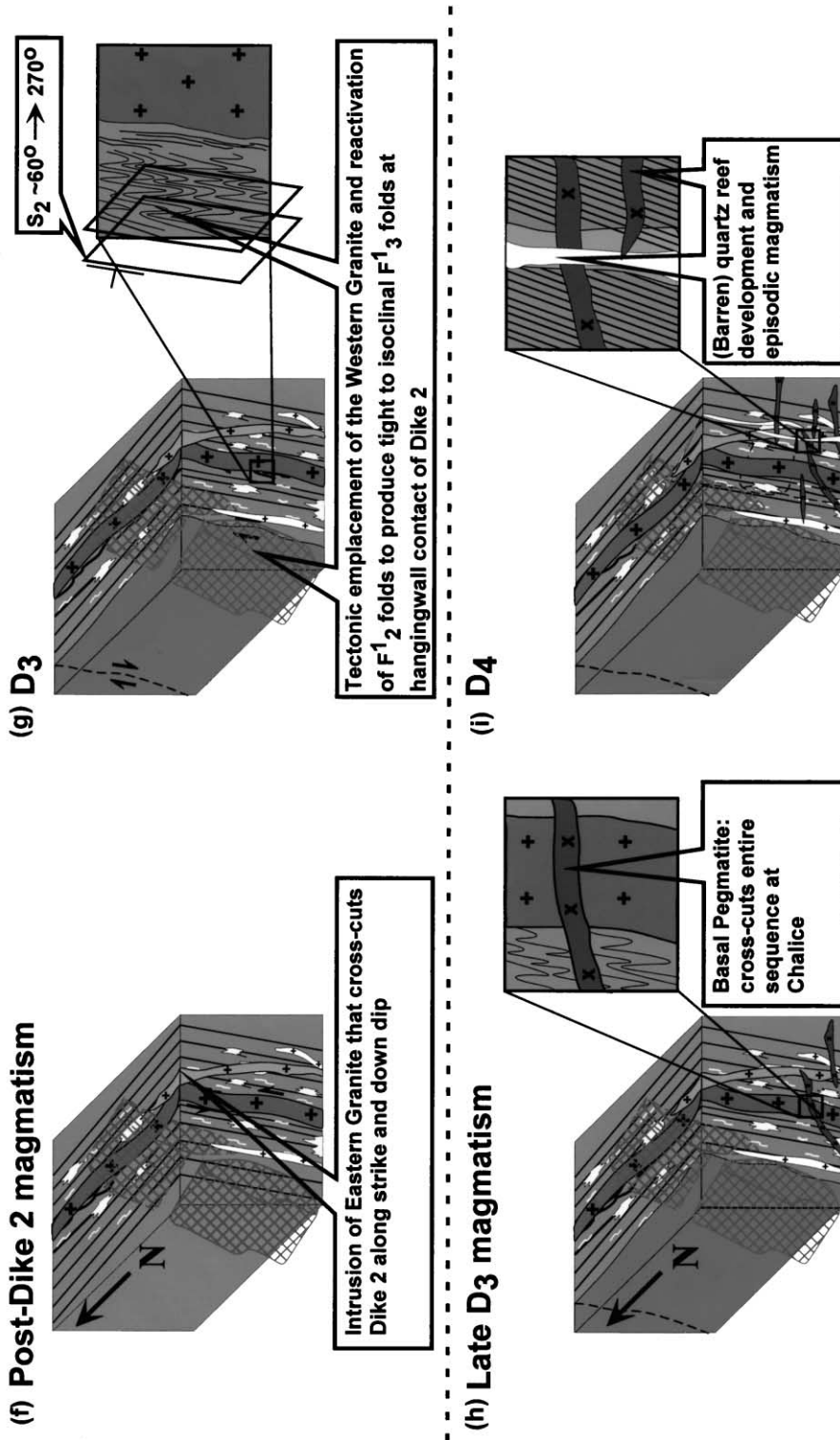


Fig. 11 (continued).



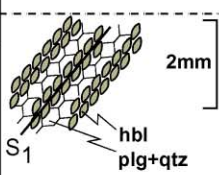
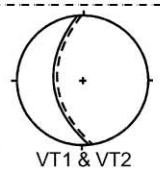
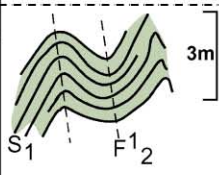
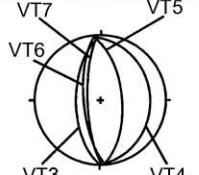
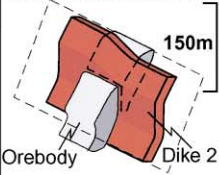
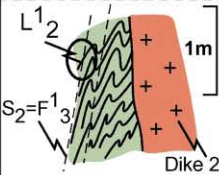
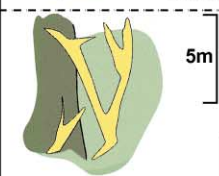
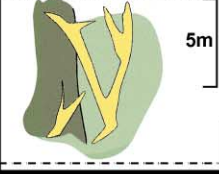
EVENT	DEFORMATION AND METAMORPHISM	REPRESENTATIVE STRUCTURE	MAGMATISM	VEINS	
				MINERALOGY	ORIENTATION
Pre-D	Mafic and ultramafic volcanism; $S_0$ form surface				
D <sub>1</sub>	<b>AMPHIBOLITE FACIES METAMORPHISM</b>			<b>Pre-gold mineralization</b>	
	Moderate to steeply dipping, NNW-striking $S_1$ foliation $S_1 = 70 \rightarrow 261$		<b>Dike 1 (late-D<sub>1</sub>)</b>		
D <sub>2</sub>	<b>MAIN STAGE GOLD MINERALIZATION</b>			<b>VT1:</b> Qtz-ab-dp-tnt-gt-Au-po-py-mt+/-cct <b>VT2:</b> Qtz,ab,dp	
	Drag folding of $S_1$ to produce asymmetric $F_2^1$ folds $F_2^1 = 25 \rightarrow 345$		<b>Regional granite domes (Pioneer Dome)</b>		
Late D <sub>2</sub>	<b>SECOND STAGE GOLD MINERALIZATION</b>			<b>VT3:</b> Qtz-Au <b>VT4:</b> Qtz-ab-dp-tnt-Au <b>VT5:</b> Act-ab-Au-dp <b>VT6:</b> Moly-Au-TeBi-sch-po-mt <b>VT7:</b> Qtz	
	Intrusion of Dike 2 ○ = plunge of orebody (25 → 345 & 18 → 182)		<b>Dike 2</b>		
D <sub>3</sub>	Local development of tight to isoclinal folds ( $F_3^1$ ), axial planar cleavage ( $S_2$ ) and an intersection lineation $L_2^1$ $S_2 = 258 \rightarrow 72$ , $F_3^1 = 25 \rightarrow 345$ $L_2^1 = 25 \rightarrow 345$		<b>Eastern Granite</b>	<b>Post-gold mineralization</b>	
					
D <sub>4</sub>	Massive quartz reefs and open-space cavity quartz growth Mean strike of quartz reefs (90 → 230)		<b>Basal Pegmatite (post-D<sub>4</sub>)</b>	<b>Post-gold mineralization</b>	

Fig. 12. Summary of the relative timing relationships between metamorphism, deformation, magmatism and gold mineralisation at the Chalice gold deposit. See Fig. 10 for abbreviations.

intersection of Dike 2 with the Main Stage orebody resulted in a deposit-scale gentle southerly plunge for medium- to low-grade mineralisation, which overprints the north–northwest plunge of high-grade shoots associated with local  $F_2^1$  folds (stereonet: Fig. 11e; longitudinal projection: Fig. 6b). Second Stage gold mineralisation, which accounts for less than 5% of the total gold budget at Chalice, was preferentially developed on the hangingwall side of, and disseminated throughout, Dike 2. Although exact timing constraints are not quantified, cross-cutting relationships indicate that the Eastern Granite intruded into the lithostratigraphic sequence, post-Dike 2 (Fig. 11f). Emplacement of the Western Granite ( $D_3$ : Fig. 11g) produced tight-to-isoclinal  $F_3^1$  folds, an associated  $S_2$  axial–planar cleavage and intersection lineation  $L_2^1$ .

A close temporal and spatial association exists between the intrusion of the Basal Pegmatite (Late  $D_4$ : Fig. 11h) and quartz reef development ( $D_5$ : Fig. 11i). Magmatism was episodic during late  $D_4$  and resulted in flat-lying pegmatites periodically truncating, and being truncated by, quartz reefs and open-space cavity quartz growth. This likely occurred during exhumation and uplift of the sequence, as open-space cavity growth is unlikely in a hypozonal setting.

## 10. Summary and conclusions

The Chalice gold deposit located in the southwestern portion of the Norseman–Wiluna greenstone belt is bounded by a massive calc-alkaline granitoid complex (Woolgangie Super Suite) to the west, and a monzogranitic pluton (Pioneer Dome) to the east. It is, therefore, sited in an environment dominated by granitoids. The mine sequence itself consists of intercalated mafic and ultramafic volcanic rocks metamorphosed to amphibolite facies grade, but at least four generations of monzogranitic dike intruded the sequence during post-peak metamorphism conditions, further emphasising the importance of granitic magmatic activity in the mine environment.

Four, in part progressive, deformation events affected the mine sequence.  $D_1$ : deposit-scale foliation ( $S_1$ ,  $\sim 70^\circ \rightarrow 261^\circ$ );  $D_2$ : local asymmetric folds ( $F_2^1$ ,  $\sim 25^\circ \rightarrow 345^\circ$ ); Late  $D_2$ : intrusion of Dike 2 and

development of associated veins;  $D_3$ : reactivation of  $D_2$  folds to produce  $F_3^1$  folds ( $\sim 25^\circ \rightarrow 345^\circ$ ), axial planar cleavage ( $S_2$ ,  $60^\circ \rightarrow 270^\circ$ ) and an intersection lineation ( $L_2^1$ ,  $25^\circ \rightarrow 345^\circ$ ); and  $D_4$ : laminated quartz reefs ( $\sim 80^\circ \rightarrow 265^\circ$ ). The mine environment is, therefore, structurally complex.

Two stages of gold mineralisation are recognised. Main and Second Stage gold mineralisation are controlled by  $D_2$  folds and the intrusion of Dike 2, respectively. Collectively, they define a stratabound orebody which grades  $\sim 6$  g/t gold and parallels the  $S_1$  fabric. As this fabric is deformed by  $D_2$  folds, the geometry of the orebody is complex. High-grade shoots (200–400 gm) plunge parallel to  $D_2$  fold axes. Medium-grade shoots (50–200 gm) are controlled by the superposition of the dike with Main Stage gold mineralisation.

Main Stage gold mineralisation, comprising  $\sim 95\%$  of the resource, is defined by variably deformed foliation-parallel veins and pervasive wall-rock alteration, both characterised by a high-temperature quartz–diopside–plagioclase–K-feldspar–titanite  $\pm$  garnet  $\pm$  hornblende  $\pm$  scheelite and biotite assemblage with accessory pyrite, pyrrhotite and magnetite. This mineralisation stage is hosted exclusively in mafic amphibolite and has a gold-dominated metal association with trace Cu and W. Free gold is locally intergrown, and in textural equilibrium, with diopside, quartz, hornblende, garnet and pyrrhotite.

Second Stage gold mineralisation,  $\sim 5\%$  of the resource, is defined by disseminated gold in Dike 2 and associated with high-temperature foliation-discordant quartz–gold, quartz–diopside–gold, actinolite–gold and molybdenite–tellurobismuthite–gold veins. This mineralisation cross-cuts Main Stage mineralisation and is developed in mafic amphibolite, the Hangingwall Ultramafic unit and Dike 2. The Au–Bi–Te–Mo–W metal association contrasts with the Au–minor Cu–W association of Main Stage mineralisation.

Main Stage gold mineralisation at Chalice is best classified as hypozonal orogenic lode–gold, when compared with intrusion-related vein gold, Phanerozoic gold-skarn and orogenic lode–gold mineralisation. Although this mineralisation event is bracketed by magmatic episodes (Woolgangie Super Suite and the Pioneer Dome), it cannot be correlated to a particular granitoid in the local environment. Thus, a distal metamorphic and/or magmatic source is implicated

for the ore fluid. Second Stage gold mineralisation is, however, atypical of hypozonal orogenic lode–gold deposits and is directly associated with the intrusion of Dike 2. It is uncertain if this event produced true magmatic gold, or represents assimilation and remobilisation of Main Stage gold during Dike 2 magmatism. However, the Au–Bi–Te–Mo–W association is very similar to that ascribed to intrusion-related gold deposits, particularly those associated with the Tombstone Plutonic Suite, strengthening the granitoid–gold connection.

Irrespective of the uncertainties concerning Main Stage mineralisation, the close association of Second Stage gold with monzogranite Dike 2 magmatism, its Au–Bi–Te–Mo–W association and the close spatial and temporal link between gold mineralisation and extended granitoid magmatism for the deposit as a whole implicate metamorphism and associated granitoids, in the genesis of the Chalice gold deposit.

### Acknowledgements

This paper forms part of a doctoral study by LAB who is the recipient of an Australian Postgraduate Award (Industry), in conjunction with Resolute Limited. Ross Kennedy and Chris Bonwick are thanked for supporting this study as well as providing access to the Chalice mine site. Damien Addison, Dean Goodwin, Peter Muccilli, Craig Pinder and Piers Reynolds are acknowledged for their assistance with logistics and discussions in the field. Discussions with Andreas Mueller greatly benefited in the understanding of the alteration systematics at Chalice. Kevin Cassidy, Cam McCuaig, John Mair, Peter van der Borgh and Roberto Weinberg are thanked for many discussions and their insight into geochemistry and structural geology. Reviews by Franco Pirajno and Peter Laznicka greatly improved the manuscript.

### References

- Archibald, N.J., 1979. Tectono-metamorphic evolution of an Archean terrain: a study of the Norseman–Widgiemoorltha granitoid-greenstone belt, Eastern Goldfields Province, Western Australia. PhD thesis, Univ. West. Aust., 200 pp. (unpublished).
- Archibald, N.J., 1998. An allochthonous model for greenstone belt evolution in the Menzies–Norseman area, Eastern Goldfields Province: Implications for gold mineralization. *Geodynamics* and gold exploration in the Yilgam. AGCRC workshop and abstracts Volume, Perth, 10–17.
- Archibald, N.J., Bettenay, L.R., Binns, R.A., Groves, D.I., Gunthorpe, R.J., 1978. The evolution of Archean greenstone terrains, Eastern Goldfields Province, Western Australia. *Precambrian Res.* 6, 103–131.
- Arndt, N.Y., Nisbet, E.G., 1982. What is a komatiite? In: Arndt, N.T., Nisbet, E.G. (Eds.), *Komatiites*. Allen & Unwin, London, pp. 19–28.
- Barnicoat, A.C., 1989. The genesis of amphibolite–facies gold deposits: a model, and the example of Fraser mine, Southern Cross. Internal Report, Key Centre for Teaching and Research in Strategic Mineral Deposits, Geology Department, The University of Western Australia, 59 pp. (unpublished).
- Bell, T.H., Duncan, A.C., 1978. A rationalized and unified shorthand terminology for lineations and fold axes in tectonites. *Tectonophysics* 47, T1–T5.
- Bloem, E.J.M., Dalstra, H., Groves, D.I., Ridley, J.R., 1994. Metamorphic and structural setting of amphibolite-hosted gold deposits between Southern Cross and Bullfinch, Southern Cross Province, Yilgam Block, Western Australia. *Ore Geol. Rev.* 9, 183–208.
- Bonwick, C.M., 1995. Discovery of the Chalice gold deposit. *New Generation Gold Mines: Case History of Discovery*. Perth 27–28 November 1995.
- Campbell, I.H., Hill, R.I., 1988. A two stage model for their formation of the granite-greenstone terrains of the Kalgoorlie–Norseman area, Western Australia. *Earth Planet. Sci. Lett.* 90, 11–25.
- Cassidy, K.F., Groves, D.I., McNaughton, N.J., 1998. Late-Archean granitoid-hosted lode gold deposits, Yilgam Craton, Western Australia: deposit characteristics, crustal architecture and implications for ore genesis. *Ore Geol. Rev.* 13, 65–102.
- Claoué-Long, J.C., Compston, W., Cowden, A., 1988. The age of the Kambalda greenstones resolved by ion-microprobe: implications for Archean dating methods. *Earth Planet. Sci. Lett.* 90, 11–25.
- Craig, J.R., Vokes, F.M., 1993. The metamorphism of pyrite and pyritic ore: an overview. Boyle-A-P (prefacer), *Sulphide Metamorphism and Deformation*. *Miner. Mag.*, vol. 57, pp. 3–18.
- Dalstra, H.J., Bloem, E.J.M., Ridley, J.R., 1998. Gold mineralization in amphibolite facies terrains and its relationship to metamorphism: example of a syn-peak metamorphic timing of gold mineralization at the Transvaal deposit, Yilgam Block, Western Australia. *Chron. Rech. Min.* 529, 3–24.
- Duncan, R.A., Russell, J.K., Hastings, N.L., Anderson, R.G., 1997. Relationships between chemical composition, physical properties and geology of the mineralized Emerald Lake pluton, Yukon: current research. *Pap. - Geol. Surv. Can.* 97-1A.
- Einaudi, M.T., 1977. Petrogenesis of the copper-bearing skarn at the Mason Valley Mine, Yerington District, NV. *Econ. Geol.* 72, 769–795.
- Einaudi, M.T., Meinert, L.D., Newberry, R.J., 1981. Skarn deposits. *Economic Geology 75th Anniversary Volume*. *Econ. Geol. Publ.*, Littleton, CO, pp. 317–391.
- Ettlinger, A.T., Meinert, L.D., Ray, G.E., 1992. Gold skarn mineralization and fluid evolution in the Nickel Plate Deposit, British Columbia. *Econ. Geol.* 87, 1541–1565.

- Goldfarb, R.J., Miller, L.D., Leach, D.L., Snee, L.W., 1997. Gold deposits in metamorphic rocks of Alaska. In: Goldfarb, R.J., Miller, L.D. (Eds.), *Mineral Deposits of Alaska*, Monograph 8. *Econ. Geol.*, vol. 9, pp. 151–190.
- Goldfarb, R.J., Phillips, G.N., Nokleberg, W.J., 1998. Tectonic setting of synorogenic gold deposits of the Pacific Rim. *Ore Geol. Rev.* 13, 185–218.
- Groves, D.I., 1993. The crustal continuum model for Late-Archean lode–gold deposits of the Yilgarn Block, Western Australia. *Miner. Deposita* 28, 366–374.
- Groves, D.I., Binns, R.A., Barrett, F.M., McQueen, K.G., 1975. Sphalerite compositions from Western Australian nickel deposits, a guide to equilibria below 300 °C. *Econ. Geol.* 70, 391–396.
- Groves, D.I., Goldfarb, R.J., Gebre-Mariam, M., Hagemann, S.G., Robert, F., 1998. Orogenic gold deposits: a proposed classification in the context of their crustal distribution and relationship to other gold deposit types. *Ore Geol. Rev.* 13, 7–27.
- Hagemann, S.G., Groves, D.I., Ridley, J.R., Vearncombe, J.R., 1992. The Archean lode gold deposits at Wiluna, Western Australia; high-level brittle-style mineralization in a strike–slip regime. *Econ. Geol.* 87, 1022–1053.
- Hagemann, S.G., Brown, P.E., Ridley, J.R., Stern, P., Fournelle, J., 1998. Ore petrology, chemistry, and timing of electrum in the Archean hypozonal Transvaal lode gold deposit, Western Australia. *Econ. Geol.* 93, 271–291.
- Hagemann, S.G., Groves, D.I., Bucci, L.A., Grainger, C.J., Bodycoat, F., Witt, W.K., 2000. Amphibolite-hosted gold: hypozonal or skarn deposits? Brazil 2000, 31st International Geological Congress, Abstracts Volume. Rio de Janeiro, Brazil, August 6–17.
- Hammond, R.L., Nisbet, B.W., 1992. Towards a structural and tectonic framework for the central Norseman–Wiluna greenstone belt, Western Australia. In: *Geol. Dept. and Univ. Extension, Univ. West. Aust. Publ.* 22, pp. 39–49.
- Hickey, R.J., 1992. The Buckhorn Mountain (Crown Jewel) gold skarn deposit, Okanogan County, Washington. *Econ. Geol.* 87, 125–141.
- Hill, R.I., Campbell, I.H., Chappell, B.W., 1992. Crustal growth, crustal reworking, and granite genesis in the south-eastern Yilgarn Block, Western Australia. *Geol. Dept. and Univ. Extension, Univ. West. Aust. Publ.* 22, pp. 203–212.
- Knight, J.T., Groves, D.I., Ridley, J.R., 1993. District-scale structural and metamorphic controls on Archean lode–gold mineralization in the amphibolite facies Coolgardie goldfield, Western Australia. *Miner. Deposita* 28, 436–456.
- Knight, J.T., Ridley, J.R., Groves, D.I., 2000. The Archean amphibolite-facies Coolgardie goldfield, Yilgarn Craton, Western Australia: nature, controls and gold field-scale patterns of hydrothermal wall-rock alteration. *Econ. Geol.* 95, 49–84.
- Kotlyar, B.B., Theodore, T.G., Singer, D.A., Moss, K., Campo, A.M., Johnson, S.D., 1998. Geochemistry of the Au-skarn environment at Copper Canyon, Battle Mountain mining district, Nevada. In: Lentz, D.R. (Ed.), *Mineralized Intrusion-Related Skarn Systems*. Short Course Handb. - Mineral. Assoc. Can., vol. 26, pp. 415–444.
- Krapez, B., Brown, S.J.A., Hand, J., Barley, M.E., Cas, R.A.F., 2000. Age constraints on recycled crustal and supracrustal sources of Archean metasedimentary sequences, Eastern Goldfields Province, Western Australia: evidence from SHRIMP zircon dating. *Tectonophysics* 322, 89–133.
- Kuyper, B.A., 1988. Geology of the McCoy gold deposit, Lander County, Nevada. In: Schafer, R.W., Cooper, J.J., Vikre, P.G. (Eds.), *Bulk Mineable Precious Metal Deposits of the Western United States*; Symposium Proceedings, pp. 173–185.
- Lang, J.R., Baker, T., Hart, C.J.R., Mortensen, J.K., 2000. An exploration model for intrusion-related gold systems. *SEG Newslett.* 40, 1–15.
- McCuaig, T.C., Kerrich, R., Groves, D.I., 1993. The nature and dimensions of regional and local gold-related hydrothermal alteration in tholeiitic metabasalts in the Norseman goldfields: the missing link in a crustal continuum of gold deposits? *Miner. Deposita* 28, 420–435.
- Meinert, L.D., 1998. A review of skarns that contain gold. In: Lentz, D.R. (Ed.), *Mineralized Intrusion-Related Skarn Systems*. Short Course Handb. - Mineral. Assoc. Can., vol. 26, pp. 359–414.
- Meinert, L.D., Hefton, K.K., Mayes, D., Tasiran, I., 1997. Geology, zonation, and fluid evolution of the Big Gossan Cu–Au skarn deposit, Ertsberg District, Irian Jaya. *Econ. Geol.* 92, 509–534.
- Miyashiro, A., 1973. *Metamorphism and Metamorphic Belts*. Allen & Unwin, London.
- Morris, P.A., 1993. Archean mafic and ultramafic volcanic rocks, Menzies to Norseman, Western Australia. *Geol. Surv. West. Aust., Rep.* 36.
- Mueller, A.G., 1991. The Savage lode magnesian skarn in the Marvel Loch gold–silver mine, Southern Cross greenstone belt, Western Australia: Part 1. Structural Setting, petrography, and geochemistry. *Can. J. Earth Sci.* 28, 659–685.
- Mueller, A.G., 1997. The Nevoria gold skarn deposit in Archean iron-formation, Southern Cross greenstone belt, Western Australia: Part 1. Tectonic setting, petrography and geochemistry. *Can. J. Earth Sci.* 28, 181–209.
- Mueller, A.G., Groves, D.I., 1991. The classification of Western Australian greenstone-hosted gold deposits according to wall-rock-alteration mineral assemblages. *Ore. Geol. Rev.* 6, 291–331.
- Mueller, A.G., Groves, D.I., Delor, C.P., 1991. The Savage lode magnesian skarn in the Marvel Loch gold–silver mine, Southern Cross greenstone belt, Western Australia: Part 2. Pressure–temperature estimates and constraints on fluid sources. *Can. J. Earth Sci.* 28, 686–705.
- Mueller, A.G., Campbell, I.H., Schiotte, L., Seigney, J.H., Layer, P.W., 1996. Constraints on the age of granitoid emplacement, metamorphism, gold mineralization, and subsequent cooling of the Archean greenstone terrane at Big Bell, Western Australia. *Econ. Geol.* 91, 896–915.
- Myers, J.S., 1993. Precambrian history of the West Australian Craton and adjacent orogens. *Annu. Rev. Earth Planet. Sci.* 21, 453–485.
- Myers, J.S., 1997. Preface: archaean geology of the Eastern Goldfields of Western Australia—regional overview. *Precambrian Res.* 83, 1–10.
- Nelson, D.R., 1995. Compilation of SHRIMP U–Pb zircon geochronology data, 1994. *Geol. Surv. West. Aust. Rec.*, vol. 1995/3.

- Nelson, D.R., 1997. Evolution of the Archaean granite–greenstone terranes of the Eastern Goldfields, Western Australia: SHRIMP U–Pb zircon constraints. *Precambrian Res.* 83, 57–81.
- Phillips, G.N., Groves, D.I., 1983. The nature of gold-bearing fluids deduced from the gold deposits of Western Australia. *Aus. J. Earth Sci.* 30, 25–39.
- Phillips, G.N., Groves, D.I., Kerrich, R., 1996. Factors in the formation of the giant Kalgoorlie gold deposit. *Ore. Geol. Rev.* 10, 295–317.
- Plyusnina, L.P., 1982. Geothermometry and geobarometry of plagioclase–hornblende bearing assemblages. *Contrib. Mineral. Petrol.* 80, 140–146.
- Ray, G.E., Dawson, K.M., 1998. Mineralized skarns in the Canadian Cordillera. In: Lentz, D.R. (Ed.), *Mineralized Intrusion-Related Skarn Systems*. Short Course Handb. - Mineral. Assoc. Can., vol. 26, pp. 475–518.
- Ridley, J.R., Groves, D.I., Hagemann, S.G., 1995. Exploration and deposit models for gold deposits in amphibolite/granulite facies terrains. *Minerals and Exploration Research Institute of Western Australia report*, 142 pp.
- Ridley, J.R., Groves, D.I., Knight, J.T., 2000. Gold deposits in amphibolite and Granulite facies terranes of the Archaean Yilgarn Craton, Western Australia: evidence and implications of synmetamorphic mineralization. *Rev. Econ. Geol.*, vol. 11, pp. 265–290.
- Sillitoe, R.H., Thompson, J.F.H., 1998. Intrusion-related vein gold deposits; types, tectono-magmatic settings and difficulties of distinction from orogenic gold deposits. *Soc. Res. Geol.* 48, 237–250.
- Spear, F.S., 1980. NaSi/CaAl exchange equilibria between plagioclase and amphibole. An empirical model. *Contrib. Mineral. Petrol.* 85, 33–41.
- Strecheisen, A., 1976. To each plutonic rocks its proper name. *Earth Sci. Rev.* 12, 1–33.
- Swager, C.P., 1997. Tectono-stratigraphy of Late Archaean greenstone terranes in the southern Eastern Goldfields, Western Australia. *Precambrian Res.* 83, 11–42.
- Swager, C.P., Witt, W.K., Griffin, T.J., Ahmat, A.L., Hunter, W.M., McGoldrick, P.J., Wyche, S., 1992. Late Archaean Granite–Greenstones of the Kalgoorlie Terrane, Yilgarn Craton, Western Australia, vol. 22. *Geol. Dept. and Univ. Extension, Univ. West. Aust. Publ.*, pp. 107–122.
- Thompson, J.F.H., Sillitoe, R.H., Baker, T., Lang, J.R., Mortensen, J.K., 1999. Intrusion-related gold deposits associated with tungsten–tin provinces. *Miner. Deposita* 34, 323–334.
- Törnebohm, A.E., 1875. *Geognostisk beskrifning ofver Persbergets Grufvefalt: Sveriges Geologiska Undersökning*. P.A. Norstedt and Sons, Stockholm, p. 21.
- Williams, P.R., Whitaker, A.J., 1993. Gneiss domes and extensional deformation in the highly mineralized Archaean Eastern Goldfields Province, Western Australia. *Ore. Geol. Rev.* 8, 141–162.
- Winkler, H.G.F., 1976. *Petrogenesis of Metamorphic Rocks*, 4th edn. Springer, New York.